JACS
JOURNAL OF THE AMERICAN CHEMICAL SOCIETY

Subscriber access provided by ISTANBUL TEKNIK UNIV

Article

Effective Concentration as a Tool for Quantitatively Addressing Preorganization in Multicomponent Assemblies: Application to the Selective Complexation of Lanthanide Cations

Gabriel Canard, Sylvain Koeller, Grald Bernardinelli, and Claude Piguet

J. Am. Chem. Soc., **2008**, 130 (3), 1025-1040 • DOI: 10.1021/ja0772290

Downloaded from http://pubs.acs.org on February 8, 2009

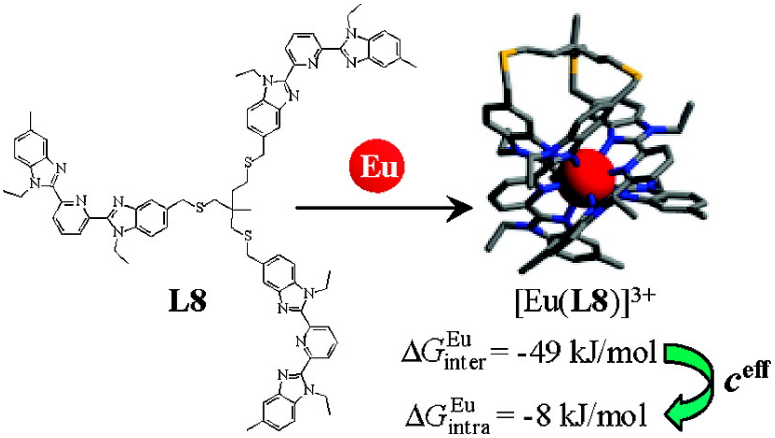

More About This Article

Additional resources and features associated with this article are available within the HTML version:

- Supporting Information
- Links to the 2 articles that cite this article, as of the time of this article download
- Access to high resolution figures
- Links to articles and content related to this article
- Copyright permission to reproduce figures and/or text from this article

View the Full Text HTML

ACS Publications
High quality. High impact.

Journal of the American Chemical Society is published by the American Chemical Society. 1155 Sixteenth Street N.W., Washington, DC 20036

J|A|C|S
ARTICLES
Published on Web 12/22/2007

Effective Concentration as a Tool for Quantitatively Addressing Preorganization in Multicomponent Assemblies: Application to the Selective Complexation of Lanthanide Cations

Gabriel Canard,[†] Sylvain Koeller,[†] Gérald Bernardinelli,[§] and Claude Piguet*,[†]

Department of Inorganic, Analytical and Applied Chemistry, University of Geneva, 30 quai E. Ansermet, CH-1211 Geneva 4, Switzerland, and Laboratory of X-ray Crystallography, University of Geneva, 24 quai E. Ansermet, CH-1211 Geneva 4, Switzerland

Received September 18, 2007; E-mail: Claude.Piguet@chiam.unige.ch

Abstract: The beneficial entropic effect, which may be expected from the connection of three tridentate binding units to a strain-free covalent tripod for complexing nine-coordinate cations (M^{z+} = Ca^{2+}, La^{3+}, Eu^{3+}, Lu^{3+}), is quantitatively analyzed by using a simple thermodynamic additive model. The switch from pure intermolecular binding processes, characterizing the formation of the triple-helical complexes $[M(\mathbf{L2})_3]^{z+}$, to a combination of inter- and intramolecular complexation events in $[M(\mathbf{L8})]^{z+}$ shows that the ideal structural fit observed in $[M(\mathbf{L8})]^{z+}$ indeed masks large energetic constraints. This limitation is evidenced by the faint effective concentrations, c^{eff}, which control the intramolecular ring-closing reactions operating in $[M(\mathbf{L8})]^{z+}$. This predominence of the thermodynamic approach over the usual structural analysis agrees with the hierarchical relationships linking energetics and structures. Its simple estimation by using a single microscopic parameter, c^{eff}, opens novel perspectives for the molecular tuning of specific receptors for the recognition of large cations, a crucial point for the programming of heterometallic f−f complexes under thermodynamic control.

Introduction

Despite attractive applications in (i) the double-sensing of protein domains and biological tissues,[1] (ii) the development of efficient homogeneous fluoroimmunoassays,[2] (iii) the efficient cleaveage of phosphodiester bonds,[3] and (iv) the design of novel materials for directional light-conversion,[4] photonic amplification,[5] nonlinear optical up-conversion,[6] and molecular four-level lasers,[7] the programmed thermodynamic incorporation of different trivalent lanthanides, Ln(III), into organized metallosupramolecular edifices remains an unsolved chemical challenge.[4] Currently, the only viable route for preparing pure heterometallic 4f−4f complexes relies on some stepwise metalation/demetalation processes operating in kinetically inert complexes possessing negatively charged ligands, such as (i) porphyrins and phthalocyanins,[8] (ii) metallocryptands,[9] (iii) podands, or (iv) macrocycles grafted with peripheral carboxylate donors.[10] However, recent contributions reporting on the quantitative preparation of heterometallic 4f−4f complexes with unsymmetrical compartmental Schiff bases[11] or with terpyridine-carboxylates[12] suggest that thermodynamic recognition may

[†] Department of Inorganic Chemistry.
[§] Laboratory of X-ray Crystallography.

(1) (a) Nitz, M.; Sherawat, M.; Franz, K. J.; Peisach, E.; Allen, K. N.; Imperiali, B. *Angew. Chem., Int. Ed.* **2004**, *43*, 3682−3685. (b) Harte, A. J.; Jensen, P.; Plush, S. E.; Kruger, P. E.; Gunnlaugsson, T. *Inorg. Chem.* **2006**, *45*, 9465−9474. (c) Martin, L. J.; Hähnke, M. J.; Nitz, M.; Wöhnert, J.; Silvaggi, N. R.; Allen, K. N.; Schwalbe, H.; Imperiali, B. *J. Am. Chem. Soc.* **2007**, *129*, 7106−7113. (d) Silvaggi, N. R.; Martin, L. J.; Schwalbe, H.; Imperiali, B.; Allen, K. N. *J. Am. Chem. Soc.* **2007**, *129*, 7114−7120.
(2) (a) Bünzli, J.-C. G. In *Metal Ions in Biological Systems*; Sigel, A., Sigel, H., Eds.; Marcel Dekker Inc.: Basel, New York, 2004; Vol 42, pp 39−75. (b) Charbonnière, L. J.; Hildebrandt, N.; Ziessel, R. F.; Löhmannsröben, H.-G. *J. Am. Chem. Soc.* **2006**, *128*, 12800−12809. (c) Lou, X.; Zhang, G.; Herrera, I.; Kinach, R.; Ornatsky, O.; Baranov, V.; Nitz, M.; Winnik, M. A. *Angew. Chem., Int. Ed.* **2007**, *46*, 6111−6114.
(3) (a) Ragunathan, K. G.; Schneider, H.-J. *Angew. Chem., Int. Ed. Engl.* **1996**, *35*, 1219−1221. (b) Liu, C.; Wang, M.; Zhang, T.; Sun, H. *Coord. Chem. Rev.* **2004**, *248*, 147−168.
(4) (a) Piguet, C.; Bünzli, J.-C. G. *Chem. Soc. Rev.* **1999**, *28*, 347−358. (b) Bünzli, J.-C. G.; Piguet, C. *Chem. Rev.* **2002**, *102*, 1897−1928. (c) Bünzli, J.-C. G.; Piguet, C. *Chem. Soc. Rev.* **2005**, *34*, 1048−1077. (d) Yang, J.; Li, G.-D.; Cao, J. J.; Li, G. H.; Chen, J.-S. *Inorg. Chem.* **2007**, *45*, 2857−2865.
(5) Oh, J. B.; Kim, Y. H.; Nah, M. K.; Kim, H. K. *J. Lumin.* **2005**, *111*, 255−264. (b) Li, L.; Jiang, W.; Pan, H.; Xu, X.; Tang, Y.; Ming, J.; Xu, Z.; Tang, R. *J. Phys. Chem. C* **2007**, *111*, 4111−4115.
(6) Auzel, F. *Chem. Rev.* **2004**, *104*, 139−173.
(7) Reisfeld, R.; Jørgensen, C. K. *Lasers and Excited States of Rare Earths*; Inorganic Chemistry Concepts; Springer-Verlag: Heidelberg, 1977; Vol 1, pp 76−79.
(8) (a) Gross, T.; Chevalier, F.; Lindsey, J. S. *Inorg. Chem.* **2001**, *40*, 4762−4774. (b) Ishikawa, N.; Kaizu, Y. *Coord. Chem. Rev.* **2002**, *226*, 93−101. (c) Schweikart, K.-H.; Malinovskii, V. L.; Yasseri, A. A.; Li, J.; Lysenko, A. B.; Bocian, D. F.; Lindsey, J. S. *Inorg. Chem.* **2003**, *42*, 7431−7446. (d) Bian, Y.; Li, L.; Wang, D.; Choi, C.-F.; Cheng, D. Y.; Zhu, P.; Li, R.; Dou, J.; Wang, R.; Pan, N.; Ng, D. K. P.; Kobayashi, N.; Jiang, J. *Eur. J. Inorg. Chem.* **2005**, 2612−2618.
(9) Dong, Y.-B.; Wang, P.; Ma, J.-P.; Zhao, X.-X.; Wang, H.-Y.; Tang, B.; Huang, R.-Q. *J. Am. Chem. Soc.* **2007**, *129*, 4872−4873.
(10) (a) Pope, S. J. A.; Kenwright, A. M.; Heath, S. L.; Faulkner, S. *Chem. Commun.* **2003**, 1550−1551. (b) Faulkner, S.; Pope, S. J. A. *J. Am. Chem. Soc.* **2003**, *125*, 10526−10527. (c) Pope, S. J. A. Kenwright, A. M.; Boote, V. A.; Faulkner, S. *Dalton Trans.* **2003**, 3780−3784. (d) Faulkner, S.; Burton-Pye, B. *Chem. Commun.* **2005**, 259−261. (e) Tremblay, M. S.; Sames, D. *Chem. Commun.* **2006**, 4116−4118.
(11) (a) Costes, J.-P.; Dahan, F.; Dupuis, A.; Lagrave, S.; Laurent, J.-P. *Inorg. Chem.* **1998**, *37*, 153−155. (b) Costes, J.-P.; Nicodème, F. *Chem. Eur. J.* **2002**, *8*, 3442−3447. (c) Costes, J.-P.; Dahan, F.; Nicodème, F. *Inorg. Chem.* **2003**, *42*, 6556−6563.

Scheme 1. Structures of the Ligands **L1**−**L7**

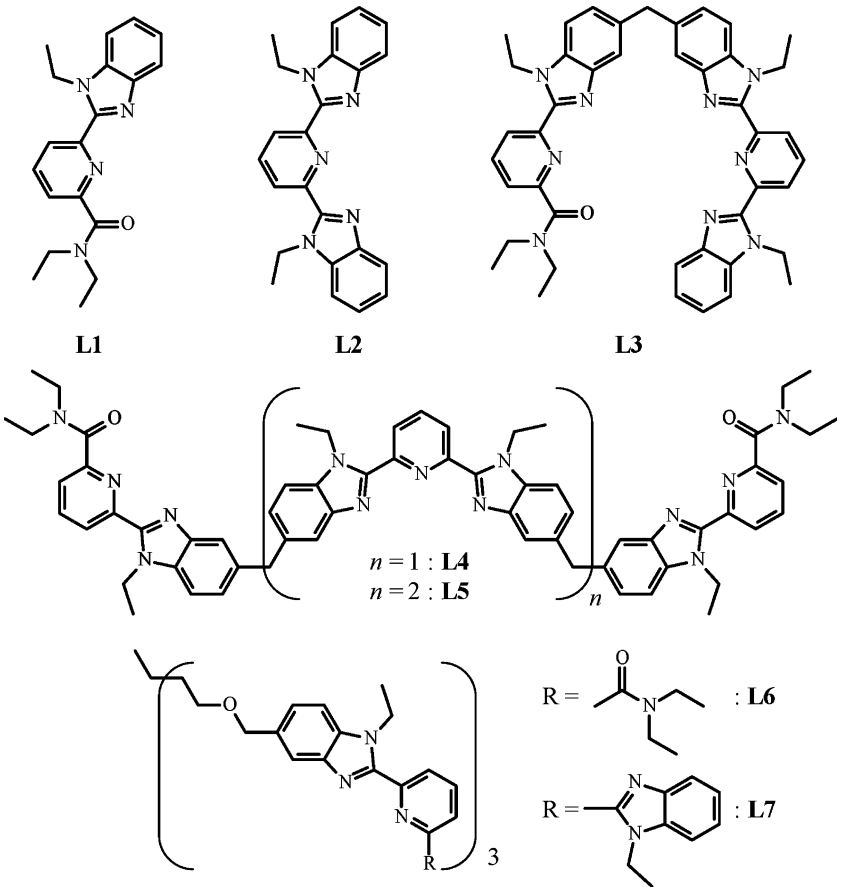

result from a judicious combination of different binding sites within the same semiflexible receptor. Following this reasoning, Bünzli and co-workers designed the neutral heterotopic bis-tridentate ligand **L3** (Scheme 1),[13] which combined a N_2O binding unit of **L1**-type, favoring the complexation of small lanthanides in $[Ln(\mathbf{L1})_3]^{3+}$ because of electrostatic driving forces,[14] and a more rigid N_3 binding unit of **L2**-type, which is known to stabilize $[Ln(\mathbf{L2})_3]^{3+}$ complexes with large lanthanides because of the operation of unfavorable interligand interactions with small cations.[15] Upon reaction of **L3** (3 equiv) with a stoichiometric amount of two different lanthanides Ln^A (1 equiv) and Ln^B (1 equiv), it was demonstrated that the thermodynamic formation of the bimetallic triple-stranded helicate $[Ln^ALn^B(\mathbf{L3})_3]^{6+}$ systematically exceeded 50% of the ligand speciation, the value predicted by the statistical binomial distribution between two equivalent coordination sites.[13] However the mixture of C_3-symmetrical head-to-head-to-head (*HHH*) and C_1-symmetrical head-to-head-to-tail (*HHT*) isomers resulting from the relative orientation of the three C_s-symmetrical ligands in $[Ln^ALn^B(\mathbf{L3})_3]^{6+}$ prevented further thermodynamic investigations of these remarkable observations.[16] The recent thorough analysis of the metal distribution occurring in the closely related D_3-symmetrical complexes $[(Ln^A)_x(Ln^B)_{3-x}(\mathbf{L4})_3]^{9+}$ ($x = 0-3$)[17] and $[(Ln^A)_x(Ln^B)_{4-x}(\mathbf{L5})_3]^{12+}$ ($x = 0-4$),[18] which also possess adjacent N_2O (**L1**-type) and N_3 (**L2**-type) tridentate binding units, but no possibility for isomerization, indicates that the microscopic affinities f^{Ln}_{N2O} and f^{Ln}_{N3} of the different tridentate chelates for a given Ln(III) are indeed very similar. Consequently, selective metallic recognition in these systems mainly relies on the modulation of the free energy of intramolecular intermetallic interaction, $\Delta E^{LnA,LnB}_{1-2}$, which is induced by subtle changes in solvation processes.[18] The rational programming of $\Delta E^{LnA,LnB}_{1-2}$ is currently inaccessible for discrete molecular objects, and this strategy has been exploited only for large (polymeric) objects, in which numerous intermetallic interactions operate.[18]

We therefore turn our attention to the exploration of the alternative concept of preorganization, measured by the effective concentration (c^{eff}),[19] for selectively coordinating Ln(III) in discrete molecular objects. In simple words, the replacement of some intermolecular connection processes with their intramo-

(12) Chen, X.-Y.; Bretonnière, Y.; Pécaut, J.; Imbert, D.; Bünzli, J.-C. G.; Mazzanti, M. *Inorg. Chem.* **2007**, *46*, 625−637.
(13) (a) André, N.; Scopelliti, R.; Hopfgartner, G.; Piguet, C.; Bünzli, J.-C. G. *Chem. Commun.* **2002**, 214−215. (b) André, N.; Jensen, T. B.; Scopelliti, R.; Imbert, D.; Elhabiri, M.; Hopfgartner, G.; Piguet, C.; Bünzli, J.-C. G. *Inorg. Chem.* **2004**, *43*, 515−529.
(14) Le Borgne, T.; Altmann, P.; André, N.; Bünzli, J.-C. G.; Bernardinelli, G.; Morgantini, P.-Y.; Weber, J.; Piguet, C. *Dalton Trans.* **2004**, 723−733.
(15) (a) Piguet, C.; Bünzli, J.-C. G.; Bernardinelli, G.; Williams, A. F. *Inorg. Chem.* **1993**, *32*, 4139−4149. (b) Petoud, S.; Bünzli, J.-C. G.; Renaud, F.; Piguet, C.; Schenk, K. J.; Hopfgartner, G. *Inorg. Chem.* **1997**, *36*, 5750−5760.
(16) Jensen, T. B.; Scopelliti, R.; Bünzli, J.-C. G. *Inorg. Chem.* **2006**, *45*, 7806−7814.
(17) Floquet, S.; Borkovec, M.; Bernardinelli, G.; Pinto, A.; Leuthold, L.-A.; Hopfgartner, G.; Imbert, D.; Bünzli, J.-C. G.; Piguet, C. *Chem.−Eur. J.* **2004**, *10*, 1091−1105.
(18) Dalla-Favera, N.; Hamacek, J.; Borkovec, M.; Jeannerat, D.; Ercolani, G.; Piguet, C. *Inorg. Chem.* **2007**, *46*, 9312−9322.

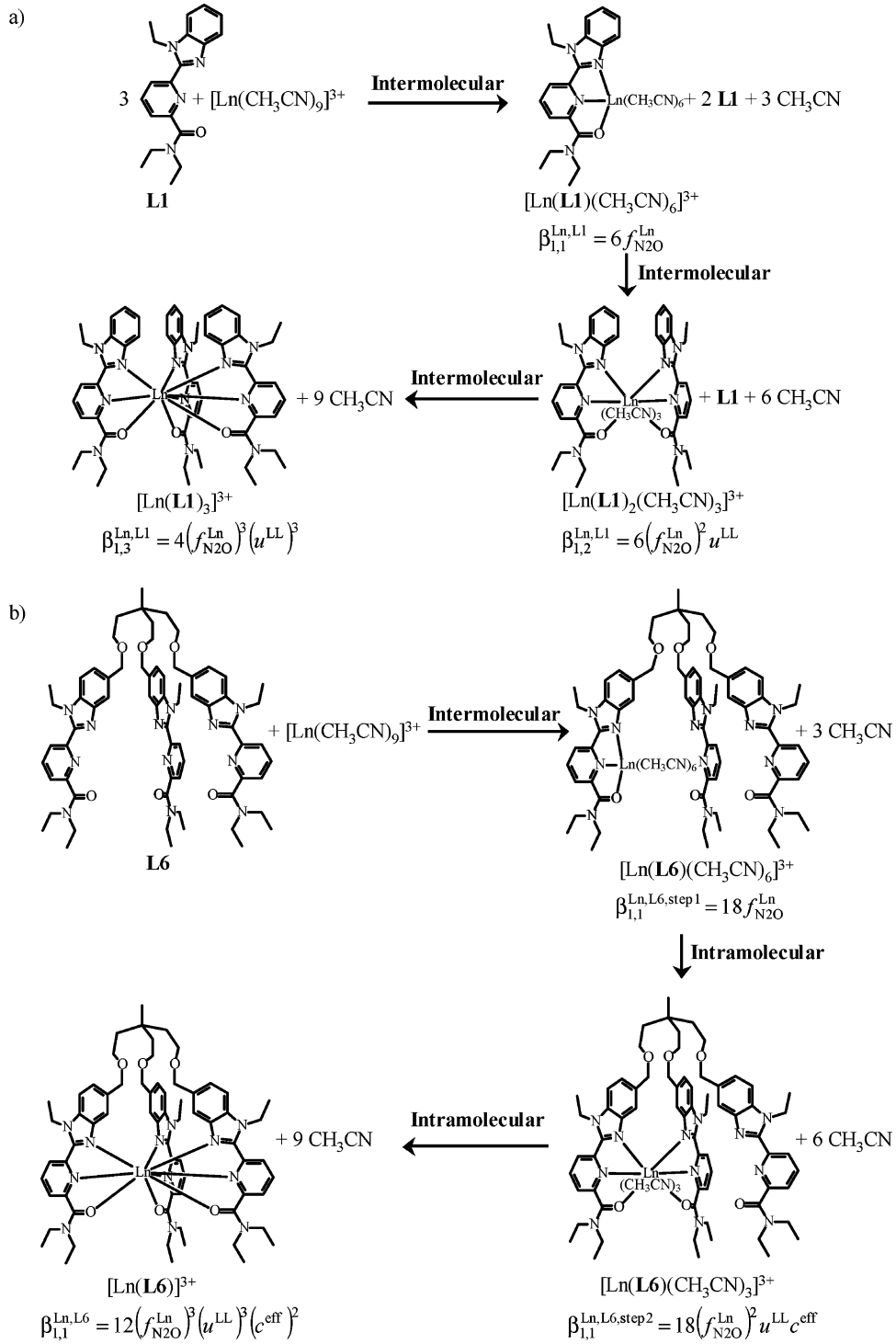

Figure 1. Successive complexation processes[24] leading to (a) *HHH*-[Ln(**L1**)$_3$]$^{3+}$ and (b) [Ln(**L6**)]$^{3+}$ with thermodynamic formation constants modeled with eq 2.[22] The statistical factors $\omega_{m,n}^{\text{chiral}} \cdot \omega_{m,n}^{\text{Ln,L}}$ are calculated in Figure S1 (Supporting Information),[23,24] and the definition of the various microscopic parameters are given in the text.[22]

lecular counterparts should improve the influence of molecular design on the complexation process, a strategy previously established for improving both stability and structural control in standard coordination complexes with multidentate ligands (i.e., the chelate effect). As a first step toward this goal, we synthesized the podand ligand **L6**, in which three tridentate N_2O binding units of **L1**-type were connected to a strain-free covalent helical tripod.[20] The complexation reactions leading to [Ln(**L1**)$_3$]$^{3+}$ or to [Ln(**L6**)]$^{3+}$ mainly differ in the successive operation of three intermolecular Metal−Ligand connection processes for [Ln(**L1**)$_3$]$^{3+}$ (Figure 1a), while the initial intermolecular binding event in [Ln(**L6**)]$^{3+}$ is followed by two intramolecular ring-closing reactions (Figure 1b).[21] The application of the simple additive thermodynamic *site binding model* (eqs 1 and 2)[22] to the complexation processes depicted in Figure 1 predicts that the cumulative formation constants for [Ln(**L1**)$_3$]$^{3+}$ (eq 3) and for [Ln(**L6**)]$^{3+}$ (eq 4) are very similar except for some slightly different statistical factors $\omega_{m,n}^{\text{chiral}} \cdot \omega_{m,n}^{\text{M,L}} = \prod_i(\sigma_{\text{chiral},j}^{\text{reactant}} \cdot \sigma_{\text{symmetry},i}^{\text{reactant}})^{n_i}/\prod_j(\sigma_{\text{chiral},j}^{\text{product}} \cdot \sigma_{\text{symmetry},i}^{\text{product}})^{n_j}$ (Figure

S1, Supporting Information, $\sigma_{symmetry}$ is the geometrical symmetry number of each species, σ_{chiral} is the symmetry number accounting for the entropy of mixing of enantiomers of each species, n_i is the stoichiometric coefficient of compound i in the considered equilibrium)[23,24] and for the introduction of the effective concentration $c^{eff} = e^{(\Delta G_{inter} - \Delta G_{intra})/RT}$ in eq 4, which corresponds to the free energy correction ($-RT \ln(c^{eff})$) required when an intermolecular binding event ($\Delta G_{inter} = -RT \ln(f_i^{M,L})$) is replaced with its intramolecular counterpart ($\Delta G_{intra} = -RT \ln(f_i^{M,L} \cdot c^{eff})$).[19]

$$m\,\mathrm{M} + n\,\mathbf{L} \rightleftharpoons [\mathrm{M}_m\mathbf{L}_n] \qquad \beta_{m,n}^{M,L} \tag{1}$$

$$\beta_{m,n}^{M,L} = e^{-(\Delta G_{m,n}{}^{M,L}/RT)} = \omega_{m,n}^{chiral} \cdot \omega_{m,n}^{M,L} \cdot \prod_{i=1}^{mn} f_i^{M,L} \cdot \prod_{i=1}^{mn-m-n+1} c_i^{eff} \cdot \prod_{i<j} u_{i,j}^{M,M} \cdot \prod_{k<l} u_{k,l}^{L,L} \tag{2}$$

$$\beta_{1,3}^{Ln,L1} = 4 \cdot (f_{N2O}^{Ln})^3 \cdot (u^{L,L})^3 \tag{3}$$

$$\beta_{1,1}^{Ln,L6} = 12 \cdot (f_{N2O}^{Ln})^3 \cdot (u^{L,L})^3 \cdot (c^{eff})^2 \tag{4}$$

In these equations, f_{N2O}^{Ln} represents the intermolecular microscopic affinity characterizing the connection of the lanthanide Ln to the N_2O binding site and $u^{L,L} = e^{-(\Delta E^{L,L}/RT)}$ is the *Boltzmann*'s factor accounting for the interligand $\Delta E^{L,L}$ free energy of interaction operating in the final complexes. Assuming that the enthalpic contributions of inter- and intramolecular complexation processes are identical when using a strain-free connector ($\Delta H_{inter} \approx \Delta H_{intra}$), the so-called effective concentration corresponds to a pure entropic term $c^{eff} = e^{(\Delta S_{intra} - \Delta S_{inter})/R}$ measuring the benefit ($c^{eff} > 1$) or drawback ($c^{eff} < 1$) of the preorganization of the binding sites.

The term $(f_{N2O}^{Ln})^3 \cdot (c^{eff})^2$ in eq 4 thus indicates that, among the three successive fixations of N_2O binding units to Ln(III), one is intermolecular (f_{N2O}^{Ln}) and two are intramolecular ($(f_{N2O}^{Ln} \cdot c^{eff})^2$). However, due to extra enthalpic terms originating from intramolecular interligand stacking interactions favoring the formation of *HHT*-[Ln(**L1**)$_3$]$^{3+}$,[14] we were unable to obtain reliable values of c^{eff} for [Ln(**L6**)]$^{3+}$. In order to prevent *HHH* ↔ *HHT* isomerization processes, we considered the podand **L7** (Scheme 1), in which three C_{2v}-symmetrical tridentate binding units of **L2**-type are connected to the strain-free tripod. However, we were unable to prepare the three ether bridges in **L7**, despite considerable synthetic efforts. In this contribution, the limiting ether connectors of **L7** are replaced with thioether bridges in **L8**, which can be easily prepared by the reaction of nucleophilic deprotonated thiols with alkyl chlorides (Scheme 2). After checking for the conservation of the structural strain-free conditions imposed by the novel tripod in [Ln(**L8**)]$^{3+}$, a thorough thermodynamic investigation eventually provides reliable and quantitative estimates for c^{eff}, which can be used as a tool for programming preorganization for the selective complexation of large cations.

Results and Discussion

Synthesis and Structural Characterization of the Podand L8 and of Its Complexes [Ca(L8)](CF$_3$SO$_3$)$_2$ and [Ln(L8)](CF$_3$SO$_3$)$_3$ (Ln = La, Nd, Eu, Gd, Tb, Lu, Y). The ligand **L8** is prepared in 25 synthetic steps from the commercially available synthons **1**, **3**, **7**, and **15** (Scheme 2). The tripod **18** is obtained according to a published multistep procedure,[20b] and it is eventually reacted with thionylchloride in pyridine to yield the electrophilic trichloride intermediate **19**.[25] The associated low yield (27%) results from competitive intra- and intermolecular condensation reactions involving partially chlorinated hydroxy tripods. The use of smooth basic conditions for hydrolyzing the ester group of **5** affords excellent yields of an unprecedented 2-pyridinecarboxylic acid **6** bearing a reactive *o*-nitroarene amide group. Its remarkable solubility in standard organic solvent allows its efficient acylation, and its coupling with **8** eventually gives **9**. Reductive cyclization followed by deprotection and activation steps yield **13**, which can be hydrolyzed under anaerobic acidic conditions to give **14** (in the presence of oxygen in neutral or basic media, the bridged disulfur dimer is rapidly formed). The ultimate coupling of deprotonated **14** with **19** under anaerobic conditions affords **L8** in fair yield.

Its ^{1}H NMR spectrum in $CDCl_3$ displays nine signals for the aromatic protons, five signals for enantiotopic methylene protons, and four signals for methyl protons in agreement with **L8** adopting dynamically average C_{3v} symmetry in solution (Figure 2a and Table S1, Supporting Information). The lack of nuclear Overhauser enhancement effect (NOE) detected within the H10−H16 and H8−H14 pairs is compatible with the standard *trans*−*trans* conformation adopted by each 2,6-bis(benzimidazol-2-yl)pyridine strand (numbering in Figure 2). Reaction of **L8** (1 equiv) with stoichiometric amounts of diamagnetic Ca(CF$_3$SO$_3$)$_2$·0.5H$_2$O (1 equiv, Figure 2b) or Ln(CF$_3$SO$_3$)$_3$·xH$_2$O (1 equiv, Ln = La, Lu, x = 1−3, Figure 2c−d, Table S1) in acetonitrile yields C_3-symmetrical [Ca(**L8**)]$^{2+}$ and [Ln(**L8**)]$^{3+}$ complexes, whereby each pair of methylene protons is diastereotopic because of the loss of the symmetry planes consequent to the helical wrapping of the three tridentate strands in the final podates. The observation of strong NOE effects within the H8−H14 and H10−H16 pairs is diagnostic for the *trans*−*trans* to *cis*−*cis* conformational change resulting from the meridional tricoordination of each 2,6-bis(benzimidazol-2-yl)pyridine unit to the central metal. The considerable low-

(19) (a) Kuhn, W. *Kolloid Z.* **1934**, *68*, 2−15. (b) Jacobson, H.; Stockmayer, W. H. *J. Chem. Phys.* **1950**, *18*, 1600−1606. (c) Flory, P. J.; Suter, U. W.; Mutter, M. *J. Am. Chem. Soc.* **1976**, *98*, 5733−5739. (d) Jencks, W. P. *Proc. Natl. Acad. Sci. U.S.A.* **1981**, *78*, 4046−4050. (e) Winnik, M. A. *Chem. Rev.* **1981**, *81*, 491−524. (f) Mandolini, L. *Adv. Phys. Org. Chem.* **1986**, *22*, 1−111. (g) Ercolani, G. *J. Phys. Chem. B* **1998**, *102*, 5699−5703. (h) Kramer, R. H.; Karpen, J. W. *Nature* **1998**, *395*, 710−713. (i) Galli, C.; Mandolini, L. *Eur. J. Org. Chem.* **2000**, 3117−3125. (j) Gargano, J. M.; Ngo, T.; Kim, J. Y.; Acheson, D. W. K.; Lees, W. J. *J. Am. Chem. Soc.* **2001**, *123*, 12909−12910. (k) Kitov, P. I.; Bundle, D. R. *J. Am. Chem. Soc.* **2003**, *125*, 16271−16284. (l) Mulder, A.; Huskens, J.; Reinhoudt, D. N. *Org. Biomol. Chem.* **2004**, *2*, 3409−3424.

(20) (a) Koeller, S.; Bernardinelli, G.; Bocquet, B.; Piguet, C. *Chem.−Eur. J.* **2003**, *9*, 1062−1074. (b) Koeller, S.; Bernardinelli, G.; Piguet, C. *Dalton Trans.* **2003**, 2395−2404.

(21) Ercolani, G. *J. Am. Chem. Soc.* **2003**, *125*, 16097−16103.

(22) (a) Hamacek, J.; Borkovec, M.; Piguet, C. *Chem.−Eur. J.* **2005**, *11*, 5217−5226. (b) Hamacek, J.; Borkovec, M.; Piguet, C. *Chem.−Eur. J.* **2005**, *11*, 5227−5237. (c) Hamacek, J.; Borkovec, M.; Piguet, C. *Dalton Trans.* **2006**, 1473−1490.

(23) Ercolani, G.; Piguet, C.; Borkovec, M.; Hamacek, J. *J. Phys. Chem. B* **2007**, *111*, 12195−12203.

(24) For the sake of simplicity in calculating symmetry numbers, we consider that Ln(III) exists in acetonitrile strictly as the tricapped trigonal prismatic complex [Ln(CH$_3$CN)$_9$]$^{3+}$, although it has been experimentally demonstrated that the main species in equilibrium in lanthanide triflate solutions in anhydrous acetonitrile are [Ln(CF$_3$SO$_3$)$_2$(CH$_3$CN)$_x$]$^+$ and [Ln(CF$_3$SO$_3$)$_3$(CH$_3$CN)$_y$]; see: Di Bernardo, P.; Choppin, G. R.; Portanova, R.; Zanonato, P. L. *Inorg. Chim. Acta* **1993**, *207*, 85−91.

(25) Baumeister, J. M.; Alberto, R.; Ortner, K.; Spingler, B.; August Schubiger, P.; Kaden, T. A. *J. Chem. Soc., Dalton Trans.* **2002**, 4143−4151.

Scheme 2. Synthesis of the Ligand **L8**

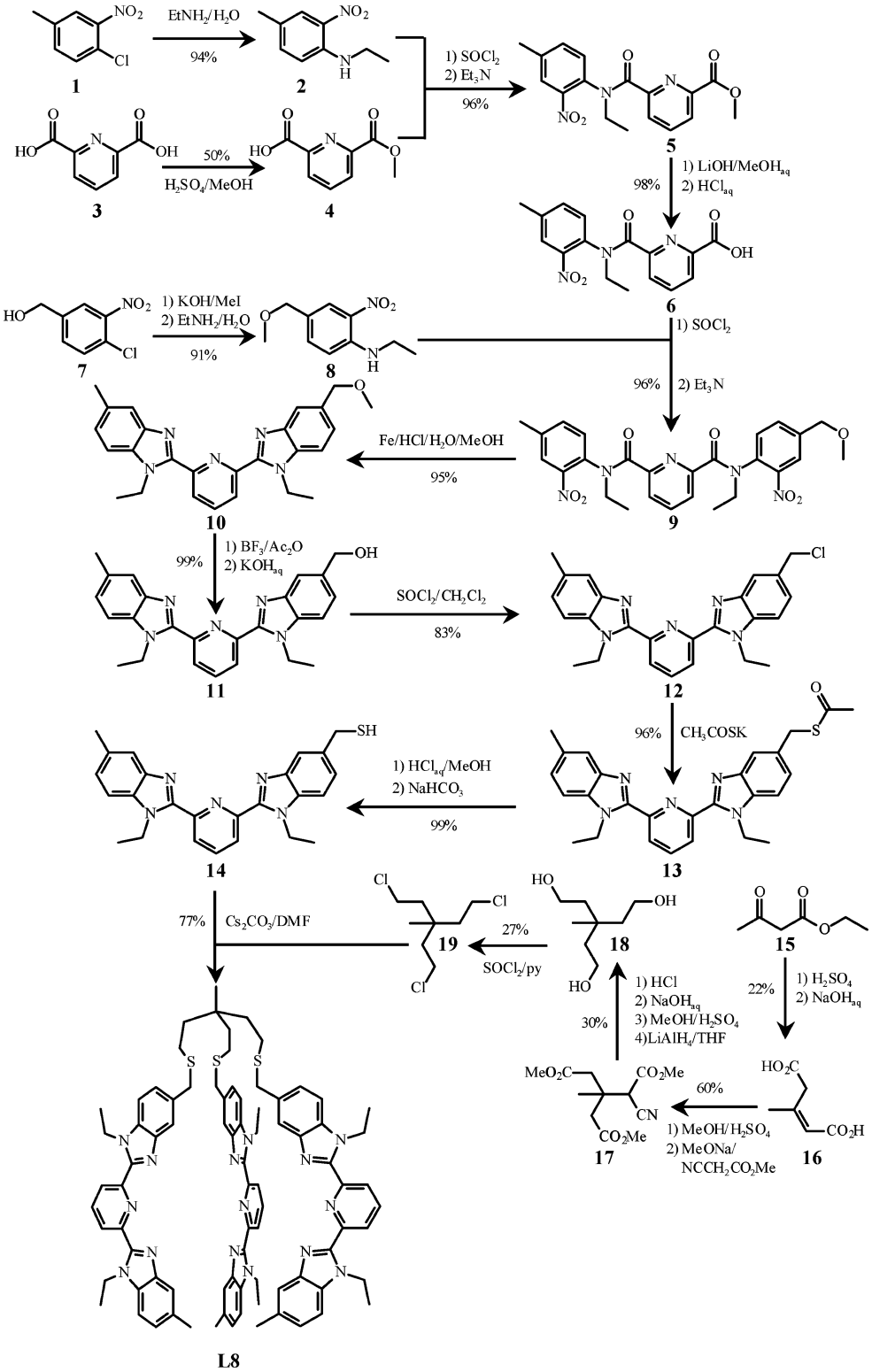

field shift affecting H5 (1.19−1.46 ppm, Table S1) and H13 (0.83−1.22 ppm, Table S1) upon complexation to diamagnetic metals in $[Ca(\mathbf{L8})]^{2+}$ and $[Ln(\mathbf{L8})]^{3+}$ (Ln = La, Lu, Y) is characteristic of the triple-helical wrapping of the strands, which puts these protons in the shielding region of the benzimidazole ring of an adjacent strand.[15] The concomitant large paramagnetic shifts $\delta_{Hi}^{Ln,para} = \delta_{Hi}^{Ln,exp} - \delta_{Hi}^{La,dia}$ calculated for H5 and H13 in $[Nd(\mathbf{L8})]^{3+}$ ($\delta_{H5}^{Nd,para} = -4.42$ ppm, $\delta_{H13}^{Nd,para} = -6.35$ ppm, Table S1) and in $[Eu(\mathbf{L8})]^{3+}$ ($\delta_{H5}^{Eu,para} = 5.24$ ppm, $\delta_{H13}^{Eu,para} = 4.07$ ppm, Table S1) further confirm their location close to the paramagnetic lanthanide in the triple-helical complex because pseudo-contact shifts depend on r_{Ln-Hi}^{-3}.[15] Diffusion of diethylether into a concentrated acetonitrile solution of $[Ca(\mathbf{L8})]^{2+}$ and $[Ln(\mathbf{L8})]^{3+}$ yields 69−94% of pale yellow microcrystalline powders whose elemental analyses correspond to $[Ca(\mathbf{L8})](CF_3SO_3)_2 \cdot 3H_2O$ and $[Ln(\mathbf{L8})](CF_3SO_3)_3 \cdot xH_2O$ (Ln = La, $x = 4$;

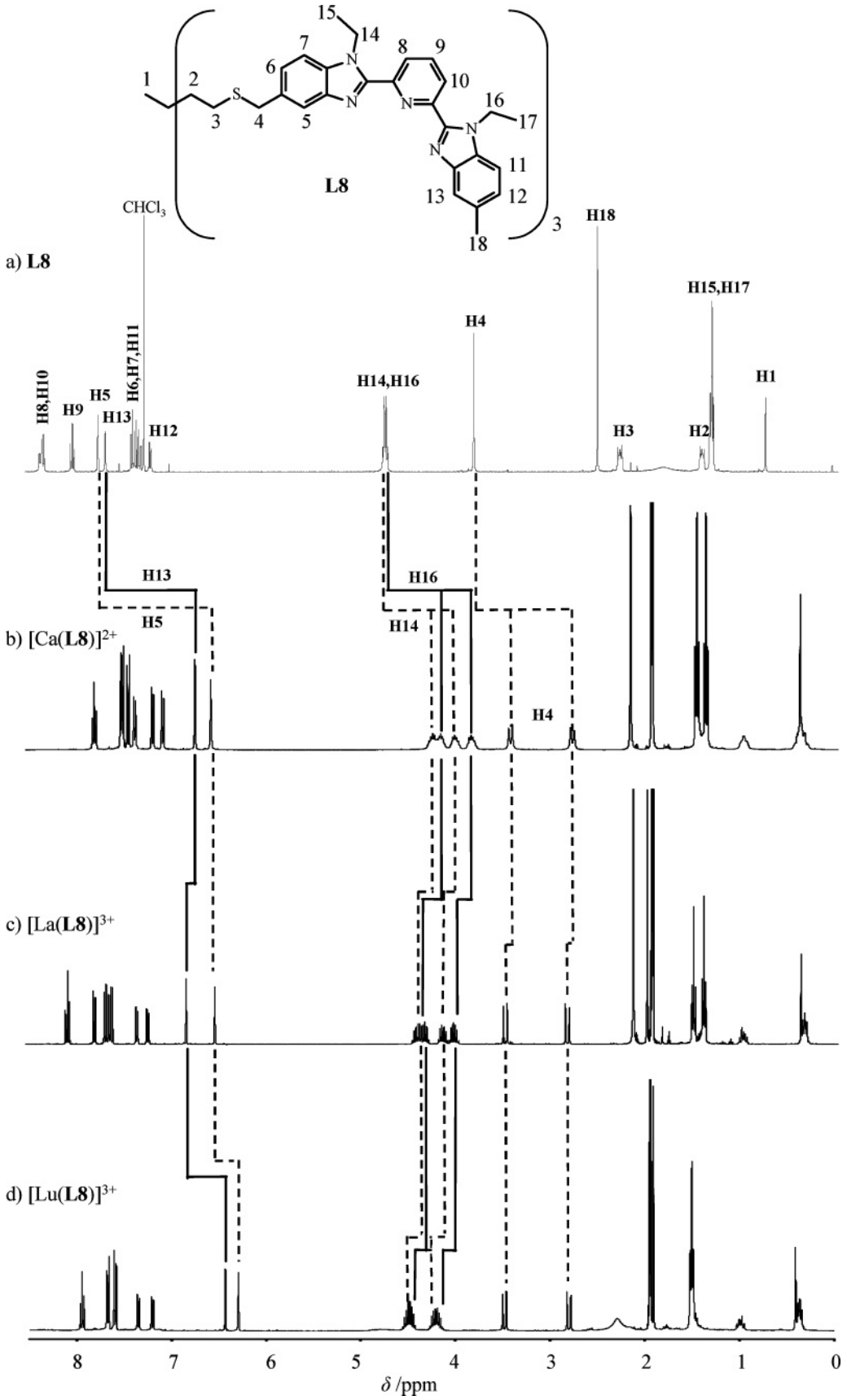

Figure 2. ^{1}H NMR spectra of (a) **L8** in $CDCl_3$ and (b) $[Ca(\mathbf{L8})]^{2+}$, (c) $[La(\mathbf{L8})]^{3+}$, and (d) $[Lu(\mathbf{L8})]^{3+}$ in CD_3CN (298 K).

Ln = Nd, $x = 4$; Ln = Eu, $x = 4$; Ln = Gd, $x = 4$; Ln = Tb, $x = 3$; Ln = Lu, $x = 4$; Ln = Y, $x = 2$, Table S2, Supporting Information).

X-ray quality plates of $[Eu(\mathbf{L8})](ClO_4)_3 \cdot 2CH_3CN \cdot C_2H_5OH \cdot 0.5H_2O$ (**20**) were obtained by slow diffusion of *tert*-butylmethylether into a concentrated solution of $[Eu(\mathbf{L8})](CF_3SO_3)_3 \cdot$

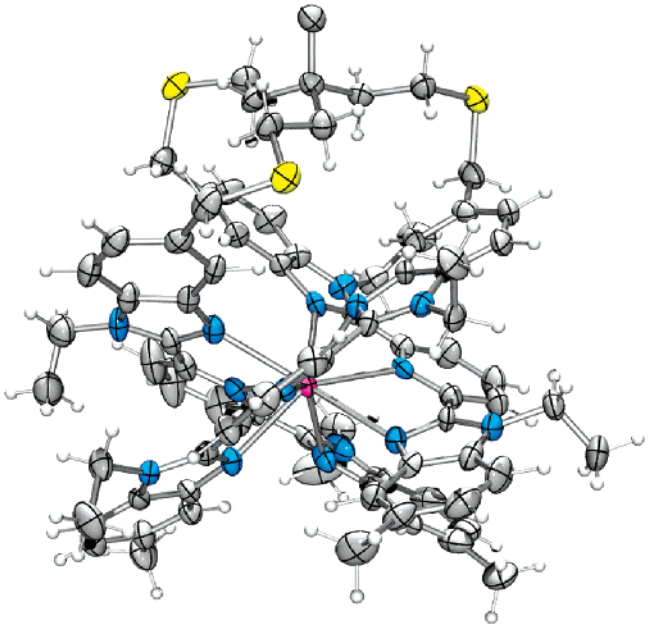

Figure 3. Perspective views of [Eu(**L8**)]$^{3+}$ perpendicular to the pseudo-threefold axis in the crystal structure of **20**. Ellipsoids are represented at the 50% probability level (C = gray, N = blue, S = yellow, H = white, Eu = violet).

Table 1. Selected Bond Distances (Å) and Angles (deg) for [Eu(**L8**)]$(ClO_4)_3$·$2CH_3CN$·C_2H_5OH·$0.5H_2O$ (**20**)

Bond Distances					
Eu−N1a	2.571(6)	Eu−N3a	2.553(5)	Eu−N4a	2.597(6)
Eu−N1b	2.614(5)	Eu−N3b	2.583(6)	Eu−N4b	2.631(6)
Eu−N1c	2.534(6)	Eu−N3c	2.559(6)	Eu−N4c	2.591(6)
Bond Angles					
N1a−Eu−N3a	63.4 (2)	N4a−Eu−N1c	74.6 (2)		
N1a−Eu−N4a	126.9 (2)	N4a−Eu−N4c	81.3 (2)		
N1a−Eu−N1b	80.0 (2)	N4a−Eu−N3c	74.8 (2)		
N1a−Eu−N3b	75.8 (2)	N1b−Eu−N3b	61.4 (2)		
N1a−Eu−N4b	75.8 (2)	N1b−Eu−N4b	124.6 (2)		
N1a−Eu−N1c	87.0 (2)	N1b−Eu−N1c	77.8 (2)		
N1a−Eu−N4c	144.0 (2)	N1b−Eu−N4c	91.4 (2)		
N1a−Eu−N3c	138.6 (2)	N1b−Eu−N3c	66.4 (2)		
N3a−Eu−N4a	63.7 (2)	N3b−Eu−N4b	64.6 (2)		
N3a−Eu−N1b	134.4 (2)	N3b−Eu−N1c	137.6 (2)		
N3a−Eu−N3b	127.1 (2)	N3b−Eu−N4c	69.4 (2)		
N3a−Eu−N4b	73.5 (2)	N3b−Eu−N3c	106.0 (2)		
N3a−Eu−N1c	74.2 (2)	N4b−Eu−N1c	147.5 (2)		
N3a−Eu−N4c	134.2 (2)	N4b−Eu−N4c	80.9 (2)		
N3a−Eu−N3c	126.9 (2)	N4b−Eu−N3c	143.4 (2)		
N4a−Eu−N1b	139.4 (2)	N1c−Eu−N4c	125.5 (2)		
N4a−Eu−N3b	145.5 (2)	N1c−Eu−N3c	63.5 (2)		
N4a−Eu−N4b	93.8 (2)	N4c−Eu−N3c	63.2 (2)		

$4H_2O$ in acetonitrile/ethanol (99.9:0.1) containing $(^nBu)_4NClO_4$ (3 equiv). The crystal structure of **20** contains nine-coordinate [Eu(**L8**)]$^{3+}$ cations, together with three noncoordinated perchlorate anions and interstitial solvent molecules. The analysis of the crystal packing shows that the [Eu(**L8**)]$^{3+}$ cations are pairwise associated about a center of inversion, thus leading to a π-stacking interaction between two benzimidazole rings belonging to the different cations of the pair (interplane angle: 0°, interplanar distance 3.54(3) Å, Figure S2, Supporting Information). Figure 3 shows a perspective view of the molecular structure of [Eu(**L8**)]$^{3+}$ in **20** (numbering scheme in Figure S3, Supporting Information), and selected bond distances and angles are collected in Table 1.

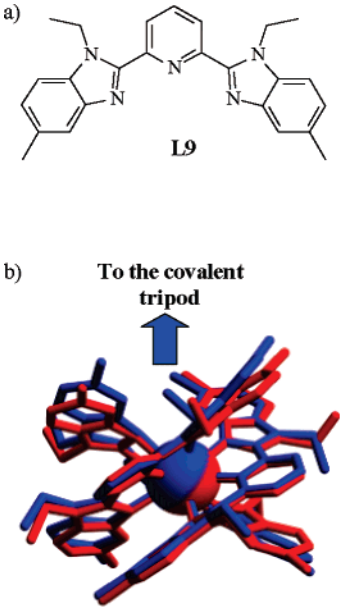

Figure 4. (a) Chemical structure of ligand **L9**. (b) Optimized superimposition of the three bound tridentate strands in [Eu(**L9**)$_3$]$^{3+}$ (red) and in [Eu(**L8**)]$^{3+}$ (blue). The upper covalent tripod in [Eu(**L8**)]$^{3+}$ (blue) has been omitted for clarity.

As inferred from ^{1}H NMR data in solution, the isolated [Eu(**L8**)]$^{3+}$ complex possesses a pseudo-threefold symmetry axis passing through the metal and the apical C1 carbon atom. The europium atom is nine-coordinate in a pseudo-tricapped trigonal prismatic arrangement produced by the three wrapped tridentate 2,6-bis(benzimidazol-2-yl)pyridine strands. Eu(III) is located close to the center of the trigonal prism and almost in the plane defined by the three capping pyridine nitrogen atoms (deviation from this plane 0.042(1) Å toward the terminal nitrogen tripod N4a,N4b,N4c). The Eu−N distances (2.534−2.631 Å, Table 1) do not deviate from the average value 2.58(3) Å. Using Shannon's definition and r(N) = 1.46 Å,[26] we calculate $R_{Eu}^{CN=9}$ = 1.121(5) Å for the ionic radius of nine-coordinate Eu(III) in [Eu(**L8**)]$^{3+}$, a value identical to (i) the standard ionic radius $R_{Eu}^{CN=9}$ = 1.120 Å expected for nine-coordinate Eu(III)[26] and (ii) $R_{Eu}^{CN=9}$ = 1.13 Å reported for [Eu(**L9**)$_3$]$^{3+}$, in which three independent **L2**-type tridentate binding units are bound to Eu(III) (Figure 4).[27] Except for some minor deviations of the six-membered aromatic rings of the benzimidazole groups connected to the sulfur tripod in [Eu(**L8**)]$^{3+}$ (Figure 4b), the arrangements of the three wrapped tridentate bound ligands are almost superimposable in [Eu(**L8**)]$^{3+}$ and [Eu(**L9**)$_3$]$^{3+}$ (Figure 4b), which provides very similar Eu(III) coordination spheres in the two complexes (Table S3, Supporting Information).

The aromatic rings are planar within experimental error (Table S4, Supporting Information), and the helical torsion responsible for the wrapping of the strands is limited to rotations about the C−C bonds connecting the pyridine and benzimidazole rings, which affords a close packing of the aromatic rings of the different strands along the pseudo-threefold axis in both complexes. We thus detect two significant intramolecular interligand π-stacking interactions in [Eu(**L8**)]$^{3+}$. The first one involves two benzimidazole rings belonging to strands a and b

(26) Shannon, R. D. *Acta Crystallogr.* **1976**, *A32*, 751−767.
(27) Piguet, C.; Bünzli, J.-C. G.; Bernardinelli, G.; Bochet, C. G.; Froidevaux, P. *J. Chem. Soc., Dalton Trans.* **1995**, 83−97.

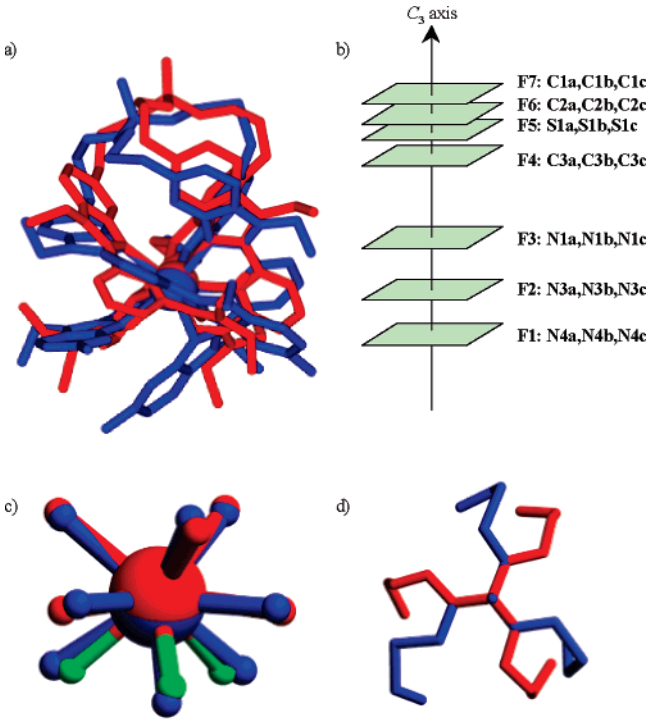

Figure 5. (a) Optimized superimposition of the podates $[Eu(\mathbf{L6})_3]^{3+}$ (red) and $[Eu(\mathbf{L8})]^{3+}$ (blue). (b) Schematic representation of the seven facial planes along the pseudo-threefold axis. (c) Optimized superimposition of the coordination spheres in $[Eu(\mathbf{L6})_3]^{3+}$ (red) and in $[Eu(\mathbf{L8})]^{3+}$ (blue). The green atoms represent the terminal oxygen atoms in $[Eu(\mathbf{L6})_3]^{3+}$. (d) View of the covalent tripods perpendicular to the C1−C2 directions in $[Eu(\mathbf{L6})_3]^{3+}$ (red) and in $[Eu(\mathbf{L8})]^{3+}$ (blue) assuming the same helicity of the three bound tridentate units about the metal in each complex.

(bza1−bzb4, interplanar angle 13.0(2)°, average interplanar distance 3.2(2) Å), and the second one operates between one benzimidazole ring of strand c and the pyridine ring of strand b (bzc4−pb3, interplanar angle 13.1(2)°, average interplanar distance 3.3(3) Å, Table S4, Supporting Information).

Finally, the superimposition of the related nine-coordinate podates $[Eu(\mathbf{L6})]^{3+}$ and $[Eu(\mathbf{L8})]^{3+}$ displays considerable discrepancies (Figure 5a) arising from (i) the different terminal donor groups (*O*-carboxamide in $[Eu(\mathbf{L6})]^{3+}$ and *N*-benzimidazole in $[Eu(\mathbf{L8})]^{3+}$, Figure 5c) and (ii) the distorted wrapping of the tripod in $[Eu(\mathbf{L8})]^{3+}$, which significantly deviates from C_3 symmetry (Figure 5d). A detailed geometrical analysis of the six successive helical portions in the podates $[Eu(\mathbf{L}i)]^{3+}$ (i = 6, 8) delimited by the seven facial planes F1−F7 depicted in Figure 5b (Table S5, Supporting Information) first shows the expected stretching of the helical pitch about the metallic sites in the F1−F2 domain when carboxamide groups in $[Eu(\mathbf{L6}]^{3+}$ are replaced with benzimidazole units in $[Eu(\mathbf{L8}]^{3+}$ (Table 2). The helical wrapping induced by the coordination of the tridentate binding units to Eu(III) in the F1−F4 domain stops within the F4−F5 domain and then restarts with the same screw direction for $[Eu(\mathbf{L8})]^{3+}$, but with the opposite screw direction for $[Eu(\mathbf{L6})]^{3+}$ (F5−F7 domain, Figure 5a and 5d, Table 2). This difference, combined with the small C3−S−C2 bond angles (98.8°−102.5°) in $[Eu(\mathbf{L8})]^{3+}$ (C3−O−C2 = 115° in $[Eu(\mathbf{L6})]^{3+}$),[20b] produces a flattening of the sulfur-containing tripod testified by the Eu···C1 distance, which amounts to 7.012(7) Å in $[Eu(\mathbf{L8})]^{3+}$ and 7.57(2) Å in $[Eu(\mathbf{L6})]^{3+}$.

We conclude from this detailed analysis of the molecular structures in the solid-state that the sulfur-containing tripod in $[Eu(\mathbf{L8})]^{3+}$ is more flexible than the analogous O-tripod in $[Eu(\mathbf{L6})]^{3+}$, which affords a less regular wrapping of the alkyl arms and an overall flattening of the capping tripod in $[Eu(\mathbf{L8})]^{3+}$. However, these minor variations do not impose any serious constraints on the wrapping of the tridentate 2,6-bis(benzimidazol-2-yl)pyridine units bound to Eu(III), which adopt almost identical arrangements in $[Eu(\mathbf{L8})]^{3+}$ and in $[Eu(\mathbf{L9})_3]^{3+}$.

Table 2. Helical Pitches P_{ij}, Linear Distances d_{ij}, and Average Twist Angle ω_{ij} along the Pseudo-C_3 Axis in the Crystal Structures of $[Eu(\mathbf{L6})](ClO_4)_3$[20b] and $[Eu(\mathbf{L8})](ClO_4)_3$

helical portion[a]	$[Eu(\mathbf{L6})](ClO_4)_3$ d_{ij}/Å	ω_{ij}/deg	P_{ij}/Å	$[Eu(\mathbf{L8})](ClO_4)_3$ d_{ij}/Å	ω_{ij}/deg	P_{ij}/Å
F1−F2[b]	1.48	57.6	9.3	1.68	53.9	11.2
F2−F3	1.71	52.1	11.8	1.65	53.3	11.2
F3−F4	3.69	60.7	21.9	3.16	64.1	17.7
F4−F5	1.38	0.07	7452	1.56	9.5	58.9
F5−F6	0.41	11.8	12.5	0.54	13.2	14.7
F6−F7	0.08	27.4	1.1	1.68	53.9	11.2

[a] Each helical portion Fi−Fj is characterized by (i) a linear extension d_{ij} defined by the separation between the facial planes, (ii) an average twist angle ω_{ij} defined by the angular rotation between the projections of Ni and Nj belonging to the same ligand strand, and (iii) its pitch P_{ij} defined as the ratio of axial over angular progressions along the helical axis. $P_{ij} = (d_{ij}/\omega_{ij}) \cdot 360$ corresponds to the length of a cylinder containing a single turn of the helix defined by the geometrical characteristics d_{ij} and ω_{ij}.[20,27] [b] F1: N4a, N4b, N4c; F2: N3a, N3b, N3c; F3: N1a, N1b, N1c; F4: C3a, C3b, C3c; F5: S1a, S1b, S1c; F6: C2a, C2b, C2c; F7: C1a, C1b, C1c.

Solution Behaviors and Thermodynamic Stabilities of the Podates $[Ca(\mathbf{L8})](CF_3SO_3)_2$ and $[Ln(\mathbf{L8})](CF_3SO_3)_3$ (Ln = La−Lu, Y except Pm). Electrospray-ionization mass spectrometric (ESI-MS) titrations of **L8** (10^{-4} M in acetonitrile) with $Ca(CF_3SO_3)_2 \cdot 0.5H_2O$ or $Ln(CF_3SO_3)_3 \cdot xH_2O$ (Ln = La−Lu, Y; x = 2−9) show the formation of $[Ca(\mathbf{L8})(CF_3SO_3)_n]^{(2-n)+}$ (n = 0, 1) and $[Ln(\mathbf{L8})(CF_3SO_3)_n]^{(3-n)+}$ (n = 0−2) as the major species, together with traces of binuclear complexes $[Ca_2(\mathbf{L8})(CF_3SO_3)_n]^{(4-n)+}$ (n = 2, 3) and $[Ln_2(\mathbf{L8})(CF_3SO_3)_n]^{(6-n)+}$ (n = 2−5, Figure 6 and Table S6, Supporting Information).

The systematic observation of a pronounced end point for M:**L8** = 1.0 combined with the detection of an isosbestic point at 347 nm for M:**L8** ≤ 1.0 during spectrophotometric titrations of **L8** (10^{-4} M in acetonitrile containing 10^{-2} M $(^nBu)_4NClO_4$) with $Ca(CF_3SO_3)_2 \cdot 0.5H_2O$ or $Ln(CF_3SO_3)_3 \cdot xH_2O$ (Ln = La−Lu, Y; x = 2−9) confirm the qualitative model established by ESI-MS and the almost exclusive formation of the podates $[M(\mathbf{L8})]^{3+}$ in this stoichiometric range (Figure 7). The absence of further evolution of the absorption spectra for M:**L8** > 1.0 with the larger cations (M = Ca, La−Dy; $R_M^{CN=9} \geq 1.079$ Å, Figure 7a) shows the conservation of the complex $[M(\mathbf{L8})]^{3+}$ in an excess of metal in these conditions. On the contrary, the smooth evolution of the absorbance observed for M:**L8** > 1.0 with small cations (M = Ho−Lu, Figure 7b) indicates the destruction of $[M(\mathbf{L8})]^{3+}$ and the formation of detectable quantities of the binuclear complexes $[M_2(\mathbf{L8})]^{6+}$ in an excess of metal.

The spectrophotometric data can be thus satisfyingly fitted to equilibrium **5** for M = Ca, La−Dy, Y and to equilibria **5** and **6** for M = Ho−Lu by using nonlinear least-squares techniques (Table 3).[28]

$$M^{z+} + \mathbf{L8} \rightleftharpoons [M(\mathbf{L8})]^{z+} \qquad \beta_{1,1}^{M,L8} \qquad (5)$$

$$2\,M^{z+} + \mathbf{L8} \rightleftharpoons [M_2(\mathbf{L8})]^{2z+} \qquad \beta_{2,1}^{M,L8} \qquad (6)$$

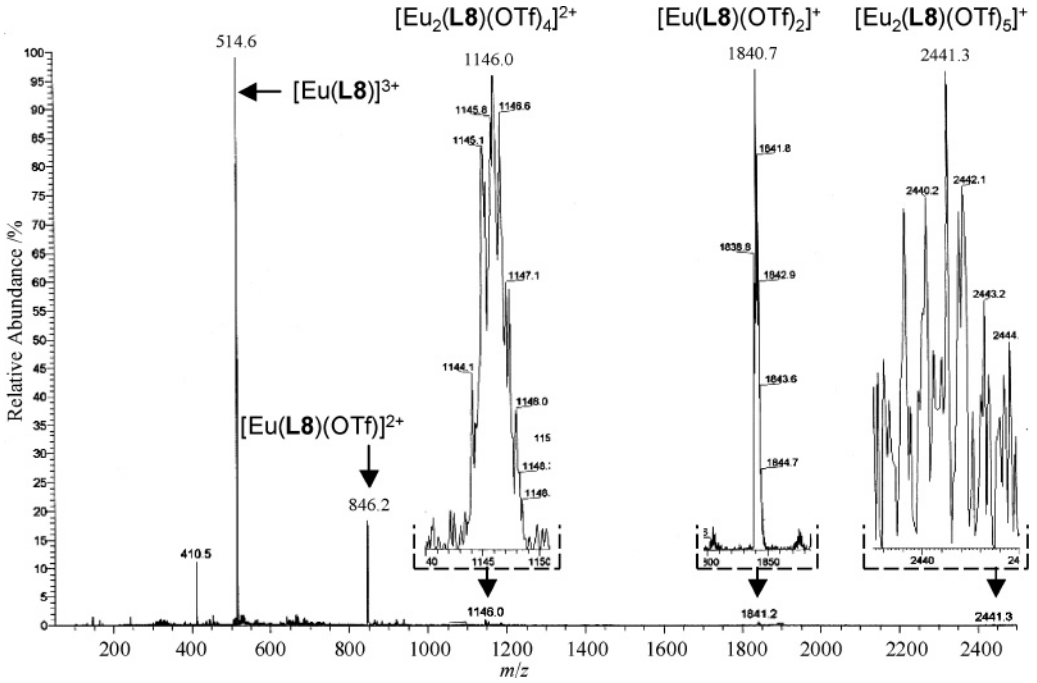

Figure 6. ESI-MS spectrum of [Eu(**L8**)](CF_3SO_3)$_3$ (10^{-4} M in acetonitrile, $OTf^- = CF_3SO_3^-$).

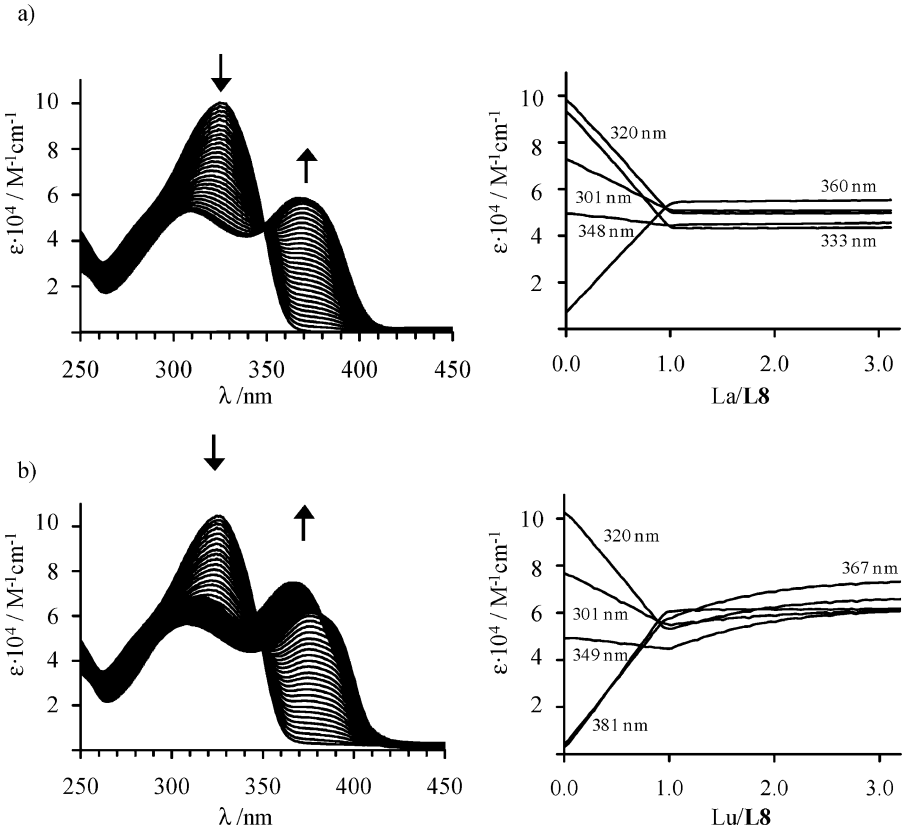

Figure 7. Variation of the absorption spectra (left) and of the molar extinctions at five different wavelengths (right) observed during the spectrophotometric titration of **L8** with (a) La(CF_3SO_3)$_3$·3.3H_2O and (b) Lu(CF_3SO_3)$_3$·1.6H_2O ($|\mathbf{L8}|_{tot} = 10^{-4}$ M, acetonitrile + 10^{-2} M (^{n}Bu)$_4$$NClO_4$, 298 K).

We first note the surprising stability of the bivalent calcium complex [Ca(**L8**)]$^{2+}$ ($\log(\beta_{1,1}^{Ca,L8}) = 8.6(8)$) with respect to that of the trivalent lanthanide complexes [Ln(**L8**)]$^{3+}$ ($7.2 \leq \log(\beta_{1,1}^{Ln,L8}) \leq 8.0$, Table 3), despite the much larger electrostatic contribution to the coordination bonds expected for the latter metals ($z^2/R_{La}^{CN=9} = 7.40$ compared with $z^2/R_{Ca}^{CN=9} = 3.39$).[26] Since the ionic radius of nine-coordinate Ca(II) ($R_{Ca}^{CN=9} = 1.18$ Å)[26] is identical to that of Pr(III) ($R_{Pr}^{CN=9} = 1.179$ Å),[26] we cannot invoke some improved matching between the ligand cavity and the metallic size. Moreover, Figure 8 shows that no size-discriminating effect can be evidenced within experimental error along the lanthanide series for [Ln(**L8**)]$^{3+}$, a behavior which contrasts with the pronounced inverse electrostatic trend reported for the formation of analogous [Ln(2,6-bis(1-methyl-

Table 3. Formation Constants of $[M_m(\mathbf{L8})]^{mz+}$ ($\log(\beta^{M,L8}_{m,1})$, $m = 1, 2$, $z = 2, 3$) and $[M(\mathbf{L2})_n]^{z+}$ ($\log(\beta^{M,L2}_{1,n})$, $n = 1-3$, $z = 2, 3$) at 298 K (Acetonitrile + 0.01 M $(^nBu)_4NClO_4$)

	M = Ca	M = La	M = Ce	M = Pr	M = Nd	M = Sm	M = Eu	M = Gd
$\log(\beta^{M,L8}_{1,1})$	8.6(8)	7.6(2)	7.2(2)	7.3(2)	7.6(2)	7.8(2)	7.2(1)	7.5(2)
$\log(\beta^{M,L2}_{1,1})$	4.4(1)	6.9(1)	–	–	–	–	9.2(5)	–
$\log(\beta^{M,L2}_{1,2})$	8.6(1)	13.0(1)	–	–	–	–	16.9(8)	–
$\log(\beta^{M,L2}_{1,3})$	11.8(3)	17.3(1)	–	–	–	–	21.8(8)	–

	M = Tb	M = Dy	M = Ho	M = Er	M = Tm	M = Yb	M = Lu	M = Y
$\log(\beta^{M,L8}_{1,1})$	7.8(2)	7.4(2)	7.9(1)	7.4(1)	7.9(1)	7.4(1)	8.0(1)	7.3(2)
$\log(\beta^{M,L8}_{2,1})$	–	–	11.7(3)	11.8(4)	11.6(1)	11.6(1)	12.7(1)	–
$\log(K^{M,L8}_{2,1})^a$	–	–	3.8(4)	4.4(5)	3.7(2)	4.2(2)	4.6(2)	–
$\log(\beta^{M,L2}_{1,1})$	–	–	–	–	–	–	9.9(3)	–
$\log(\beta^{M,L2}_{1,2})$	–	–	–	–	–	–	17.7(5)	–
$\log(\beta^{M,L2}_{1,3})$	–	–	–	–	–	–	23.4(7)	–

[a] Second successive stability constant $\log(K^{M,L8}_{2,1}) = \log(\beta^{M,L8}_{2,1}) - \log(\beta^{M,L8}_{1,1})$.

benzimidazol-2-yl)pyridine)$_3$]$^{3+}$ complexes.[15] In this context, the transformation of the podates $[Ln(\mathbf{L8})]^{3+}$ into the binuclear complexes $[Ln_2(\mathbf{L8})]^{6+}$ in an excess of metal can be safely assigned to an extra stabilization of the binuclear complexes with small cations. We also note that the replacement of the three terminal carboxamide goups in $[Ln(\mathbf{L6})]^{3+}$ with benzimidazole units in $[Ln(\mathbf{L8})]^{3+}$ has only a minor impact on the stability constants measured in the same solvent (Figure 8),[20] an observation which again contrasts with the inadequate[29] but commonly accepted rule that trivalent lanthanides should display enthalpic preferences for O-donor ligands.

A parallel ^{1}H NMR titration of **L8** (10^{-2} M in CD_3CN) with $Lu(CF_3SO_3)_3{\cdot}1.6H_2O$ shows the formation of the C_3-symmetrical podate $[Lu(\mathbf{L8})]^{3+}$ (Figure 9a), followed by its successive transformation into $[Lu_2(\mathbf{L8})]^{6+}$ and $[Lu_3(\mathbf{L8})]^{9+}$, the two latter complexes being labile on the ^{1}H NMR time scale (Figure 9b and c). In an excess of metal (Lu:**L8** = 4.0), the quantity of $[Lu_2(\mathbf{L8})]^{6+}$ becomes negligible and the exchange process does not affect the ^{1}H NMR spectrum of $[Lu_3(\mathbf{L8})]^{9+}$ (Figure 9d).[30] The conservation of the threefold axis (a total of 18 ^{1}H NMR signals are detected), combined with the deshielding of the protons H5 and H13 and the observation of enantiotopic methylene protons H2, H3, H4, H14, and H16 in $[Lu_3(\mathbf{L8})]^{9+}$, indicates the formation of a nonhelical dynamically averaged C_{3v}-symmetry for this trinuclear complex on the NMR time scale. Interestingly, the speciation found by NMR suggests values of $\log(\beta^{Lu,L8}_{2,1})$ and $\log(\beta^{Lu,L8}_{3,1})$ much larger than those estimated by spectrophotmetric titrations, a discrepancy which can be attributed to the effect of the larger ionic strength operating during the NMR experiment, which is known to favor the formation of highly charged complexes.

Thermodynamic Model and Rationalization of the Complexation Process. The application of the *site binding model* (eq 2)[22] to equilibria 5−10 gives eqs 11−16, whereby f^M_{N3} represents the microscopic affinity, including desolvation, characterizing the intermolecular connection of the metal M to the N_3 binding site (assumed to be identical for **L2** and **L8**); $u^{L,L} = e^{-(\Delta E^{L,L}/RT)}$ and $u^{M,M} = e^{-(\Delta E^{M,M}/RT)}$ are the *Boltzmann*'s factors accounting for, respectively, the intramolecular interligand $\Delta E^{L,L}$ and intermetallic $\Delta E^{M,M}$ free energies of interaction operating in the final complexes; and $c^{eff} = e^{(\Delta G_{inter} - \Delta G_{intra})/RT}$ is the effective concentration measuring the energetic effect of preorganization on intramolecular connection processes. The statistical factors $\omega^{chiral}_{m,n} \cdot \omega^{M,L}_{m,n}$ are calculated in Figure S4 (Supporting Information)[23] by using the symmetry point groups assigned to each complex in Figure 10.

$$M^{z+} + \mathbf{L8} \rightleftharpoons [M(\mathbf{L8})]^{z+} \qquad \beta^{M,L8}_{1,1} \qquad (5)$$

$$2\,M^{z+} + \mathbf{L8} \rightleftharpoons [M_2(\mathbf{L8})]^{2z+} \qquad \beta^{M,L8}_{2,1} \qquad (6)$$

$$3\,M^{z+} + \mathbf{L8} \rightleftharpoons [M_3(\mathbf{L8})]^{3z+} \qquad \beta^{M,L8}_{3,1} \qquad (7)$$

$$M^{z+} + \mathbf{L2} \rightleftharpoons [M(\mathbf{L2})]^{z+} \qquad \beta^{M,L2}_{1,1} \qquad (8)$$

$$M^{z+} + 2\,\mathbf{L2} \rightleftharpoons [M(\mathbf{L2})_2]^{z+} \qquad \beta^{M,L2}_{1,2} \qquad (9)$$

$$M^{z+} + 3\,\mathbf{L2} \rightleftharpoons [M(\mathbf{L2})_3]^{z+} \qquad \beta^{M,L2}_{1,3} \qquad (10)$$

$$\beta^{M,L8}_{1,1} = 12 \cdot (f^M_{N3})^3 \cdot (u^{L,L})^3 \cdot (c^{eff})^2 \qquad (11)$$

$$\beta^{M,L8}_{2,1} = 108 \cdot (f^M_{N3})^3 \cdot u^{L,L} \cdot c^{eff} \cdot u^{M,M} \qquad (12)$$

$$\beta^{M,L8}_{3,1} = 216 \cdot (f^M_{N3})^3 \cdot (u^{M,M})^3 \qquad (13)$$

$$\beta^{M,L2}_{1,1} = 6 \cdot f^M_{N3} \qquad (14)$$

$$\beta^{M,L2}_{1,2} = 12 \cdot (f^M_{N3})^2 {\cdot} u^{L,L} \qquad (15)$$

$$\beta^{M,L2}_{1,3} = 16 \cdot (f^M_{N3})^3 {\cdot} (u^{L,L})^3 \qquad (16)$$

If we focus on the four easily accessible thermodynamic constants $\beta^{M,L8}_{1,1}$ (eq 5), $\beta^{M,L2}_{1,1}$ (eq 8), $\beta^{M,L2}_{1,2}$ (eq 9), and $\beta^{M,L2}_{1,3}$ (eq 10), we obtain a set of four equations (eqs 11, 14−16) containing only three parameters f^M_{N3}, $u^{L,L}$, and c^{eff} to be fitted. We have thus performed spectrophotometric titrations of **L2** (10^{-4} M in acetonitrile containing 10^{-2} M $(^nBu)_4NClO_4$) with $Ca(CF_3SO_3)_2{\cdot}0.5H_2O$ or $Ln(CF_3SO_3)_3{\cdot}xH_2O$ (Ln = La, Eu and Lu; $x = 1-4$), which display the usual successive formation of the three complexes $[Ln(\mathbf{L2})_n]^{3+}$ ($n = 1-3$, Figure S5, Supporting Information).[15] Nonlinear least-square fits of these spectrophotometric data[28] provides the formation constants $\beta^{M,L2}_{1,n}$ col-

(28) (a) Gampp, H.; Maeder, M.; Meyer, C. J.; Zuberbühler, A. *Talanta* **1985**, *32*, 1133−1139. (b) Gampp, H.; Maeder, M.; Meyer, C. J.; Zuberbühler, A. *Talanta* **1986**, *33*, 943−951.
(29) Senegas, J.-M.; Bernardinelli, G.; Imbert, D.; Bünzli, J.-C. G.; Morgantini, P.-Y.; Weber, J.; Piguet, C. *Inorg. Chem.* **2003**, *42*, 4680−4695.
(30) Pons, M.; Millet, O. *Prog. Nucl. Magn. Reson. Spectrosc.* **2001**, *38*, 267−324.

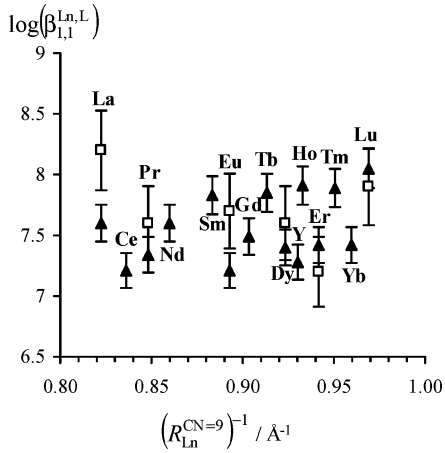

Figure 8. Plot of $\log(\beta_{1,1}^{\mathrm{Ln,L8}})$ (▲) and $\log(\beta_{1,1}^{\mathrm{Ln,L6}})$ (□)[20b] as a function of the inverse of the nine-coordinate ionic radii $(R_{\mathrm{Ln}}^{\mathrm{CN=9}})^{-1}$.

lected in Table 3. For each cation Ca^{2+}, La^{3+}, Eu^{3+}, and Lu^{3+}, we can thus easily estimate $f_{\mathrm{N3}}^{\mathrm{M}}$, $u^{\mathrm{L,L}}$, and c^{eff} by using multilinear least-squares fits of eqs 11, 14−16 in their logarithmic forms (Table 4). The quality of the fits is excellent (agreement factors $AF_{\mathrm{M}} = 0.003-0.016$, Table 4),[31] and the formation constants $\log(\beta_{1,1}^{\mathrm{M,L8,calcd}})$ and $\log(\beta_{1,n}^{\mathrm{M,L2,calcd}})$ computed by introducing the fitted microscopic parameters in eqs 11, 14−16 closely match the experimental data (Table S7, Supporting Information).

The only favorable driving force accompanying the complexation of the tridentate 2,6-bis(benzimidazol-2-yl)pyridine units to Ca(II) or Ln(III) results from the intermolecular metal−ligand connection process ($-51 \leq \Delta G_{\mathrm{inter}}^{\mathrm{M}} \leq -21$ kJ/mol, Table 4), which includes the change in solvation occurring in the first coordination sphere of the metal.[22] As expected,[32] $\Delta G_{\mathrm{inter}}^{\mathrm{M}}$ becomes more favorable (i.e., more negative, $-35 \geq \Delta G_{\mathrm{inter}}^{\mathrm{Ln}} \geq -51$ kJ/mol) with increasing electrostatic factors $z^2/R_{\mathrm{M}}^{\mathrm{CN=9}}$ (M = Ca: 3.39; M = La: 7.40; M = Eu: 8.04; M = Lu: 8.72 eu/Å^{-1}). The value for Ln = Eu, $\Delta G_{\mathrm{inter}}^{\mathrm{Eu}} = -49(2)$ kJ/mol is of the same order of magnitude as that for $\Delta G_{\mathrm{inter}}^{\mathrm{Eu}} = -30$ kJ/mol previously reported for the same tridentate N_3 unit connected to different spacers in self-assembled triple-stranded helicates $[Ln_3(\mathbf{L4})_3]^{9+}$ and $[Ln_4(\mathbf{L5})_3]^{9+}$ in pure acetonitrile.[22,33] The minor anticooperative interligand interactions $1 \leq \Delta E^{\mathrm{L,L}} \leq 10$ kJ/mol (Table 4) result from the successive fixation of electron-rich N_3 binding units to hard cations, which stepwise reduces the global charge of the metallic center by polarization.[22] Obviously, this effect is more pronounced when the total charge increases, for instance in going from Ca^{2+} to Ln^{3+}, and it reaches $\Delta E^{\mathrm{L,L}} = 10$ kJ/mol for Ln = Eu^{3+}, a value which fairly matches 8(2) kJ/mol previously reported in triple-stranded helicates.[22,33] However, the dramatic 60−80% decrease of the absolute affinity of the N_3 site for the metal, which is observed when the intermolecular connection process is replaced with its intramolecular counterpart ($-12 \leq \Delta G_{\mathrm{intra}}^{\mathrm{M}} = (\Delta G_{\mathrm{inter}}^{\mathrm{M}} + \Delta G_{\mathrm{corr}}^{\mathrm{M}}) \leq -8$ kJ/mol, Table 4), represents the most striking feature of this contribution. It implies that the favorable entropic chelate effect accompanying the fixation of the second and third tridentate binding units to the metal in $[Ln(\mathbf{L8})]^{3+}$ is more than balanced by unfavorable constraints occurring in the covalent tripod during the complexation process. This effect escapes detection in the solid state because the criteria of the superimposable strands observed in the crystal structures of $[Ln(\mathbf{L8})]^{3+}$ and $[Ln(\mathbf{L9})]^{3+}$ (Figure 4b) does not refer to the energy change accompanying the formation of the complexes from the separated ligands and metals. In contrast to the intermolecular connection processes $\Delta G_{\mathrm{inter}}^{\mathrm{Ln}}$, its intramolecular counterpart $\Delta G_{\mathrm{intra}}^{\mathrm{Ln}}$ is insensitive to the variation of the electrostatic effect along the lanthanide series, a phenomenon which can be assigned to increasing constraints operating in the tripod when the three strands wrap about small metal ions ($\Delta G_{\mathrm{corr}}^{\mathrm{Ln}}$ increases from 27 kJ/mol in $[La(\mathbf{L8})]^{3+}$ to 43 kJ/mol in $[Lu(\mathbf{L8})]^{3+}$, Table 4). The latter unfavorable contribution affecting the complexation of small lanthanides in $[Ln(\mathbf{L8})]^{3+}$ is responsible for the unwrapping of the strands and the detection of competitive polynuclear complexes $[Ln_2(\mathbf{L8})]^{6+}$ and $[Ln_3(\mathbf{L8})]^{9+}$, in which the intramolecular connections are stepwise replaced with more favorable intermolecular processes. In this context, the combination of eq 12 with the previous set of eqs 11, 14−16 for Lu(III) allows the estimation of the intermetallic interaction $\Delta E^{\mathrm{Lu,Lu}} = 42(1)$ kJ/mol operating in $[Lu_2(\mathbf{L8})]^{6+}$. Introducing this strongly repulsive parameter in eq 13 affords $\log(\beta_{3,1}^{\mathrm{M,L8}}) = 7.6$, which explains the low stability of the complex $[Lu_3(\mathbf{L8})]^{9+}$ and its exclusive detection at high concentration and in an excess of metal (^{1}H NMR titration). However, this intermetallic interaction parameter $\Delta E^{\mathrm{Lu,Lu}}$ reflects a delicate balance between considerable intramolecular intermetallic electrostatic repulsions and huge changes in solvation accompanying the stepwise transformation of $[Lu(\mathbf{L8})]^{3+}$ into $[Lu_2(\mathbf{L8})]^{6+}$ and $[Lu_3(\mathbf{L8})]^{9+}$. Its detailed interpretation will be delayed until reliable solvation energies will be available for these two complexes in solution.[34]

Experimental Section

Chemicals were purchased from Fluka AG and Aldrich and used without further purification unless otherwise stated. Ethyl-(4-methyl-2-nitro-phenyl)amine (**2**),[35] pyridine-2,6-dicarboxylic acid monomethyl ester (**4**),[36] ethyl-(4-methoxymethyl-2-nitro-phenyl)amine (**8**),[37] 1,5-dihydroxy-3-(2-hydroxy-ethyl)-3-methylpentane (**18**),[20b] and 1,5-dichloro-3-(2-chloro-ethyl)-3-methylpentane (**19**)[25] were prepared according to literature procedures. The trifluoromethanesulfonate salts $Ln(CF_3SO_3)_3 \cdot xH_2O$ (Ln = La−Lu, Y, x =1−9) were prepared from the corresponding oxides (Aldrich, 99.99%).[38] The Ln content of solid salts was determined by complexometric titrations with Titriplex III (Merck) in the presence of urotropine and xylene orange.[39] Acetonitrile and dichloromethane were distilled over calcium hydride. Thin layer chromatography (TLC) used silicagel plates Merck 60 F_{254}, and Fluka silica gel 60 (0.04−0.063 mm) was used for preparative column chromatography.

Preparation of 6-[Ethyl-(4-methyl-2-nitro-phenyl)-carbamoyl]-pyridine-2-carboxylic Acid Methyl Ester (5). Pyridine-2,6-dicar-

(31) Willcott, M. R.; Lenkinski, R. E.; Davis, R. E. *J. Am. Chem. Soc.* **1972**, *94*, 1742−1744.
(32) Choppin, G. R. In *Lanthanide Probes in Life, Chemical and Earth Sciences*; Bünzli, J.-C.G., Choppin, G. R., Eds.; Elsevier Publishing Co.: Amsterdam, 1989; Chapter 1.
(33) Zeckert, K.; Hamacek, J.; Senegas, J.-M.; Dalla-Favera, N.; Floquet, S.; Bernardinelli, G.; Piguet, C. *Angew. Chem., Int. Ed.* **2005**, *44*, 7954−7958.
(34) Canard, G.; Piguet, C. *Inorg. Chem.* **2007**, *46*, 3511−3522.
(35) Senegas, J.-M.; Koeller, S.; Bernardinelli, G.; Piguet, C. *Chem. Commun.* **2005**, 2235−2237.
(36) Johansen, J. E.; Christie, B. D.; Rapoport, H. *J. Org. Chem.* **1981**, *46*, 4914−4920.
(37) Nozary, H.; Piguet, C.; Tissot, P.; Bernardinelli, G.; Bünzli, J.-C. G.; Deschenaux, R.; Guillon, D. *J. Am. Chem. Soc.* **1998**, *120*, 12274−12288.
(38) Desreux, J. F. In *Lanthanide Probes in Life, Chemical and Earth Sciences*; Bünzli, J.-C.G., Choppin, G. R., Eds.; Elsevier Publishing Co.: Amsterdam, 1989; Chapter 2.
(39) Schwarzenbach, G. *Complexometric Titrations*; Chapman & Hall: London, 1957; p 8.

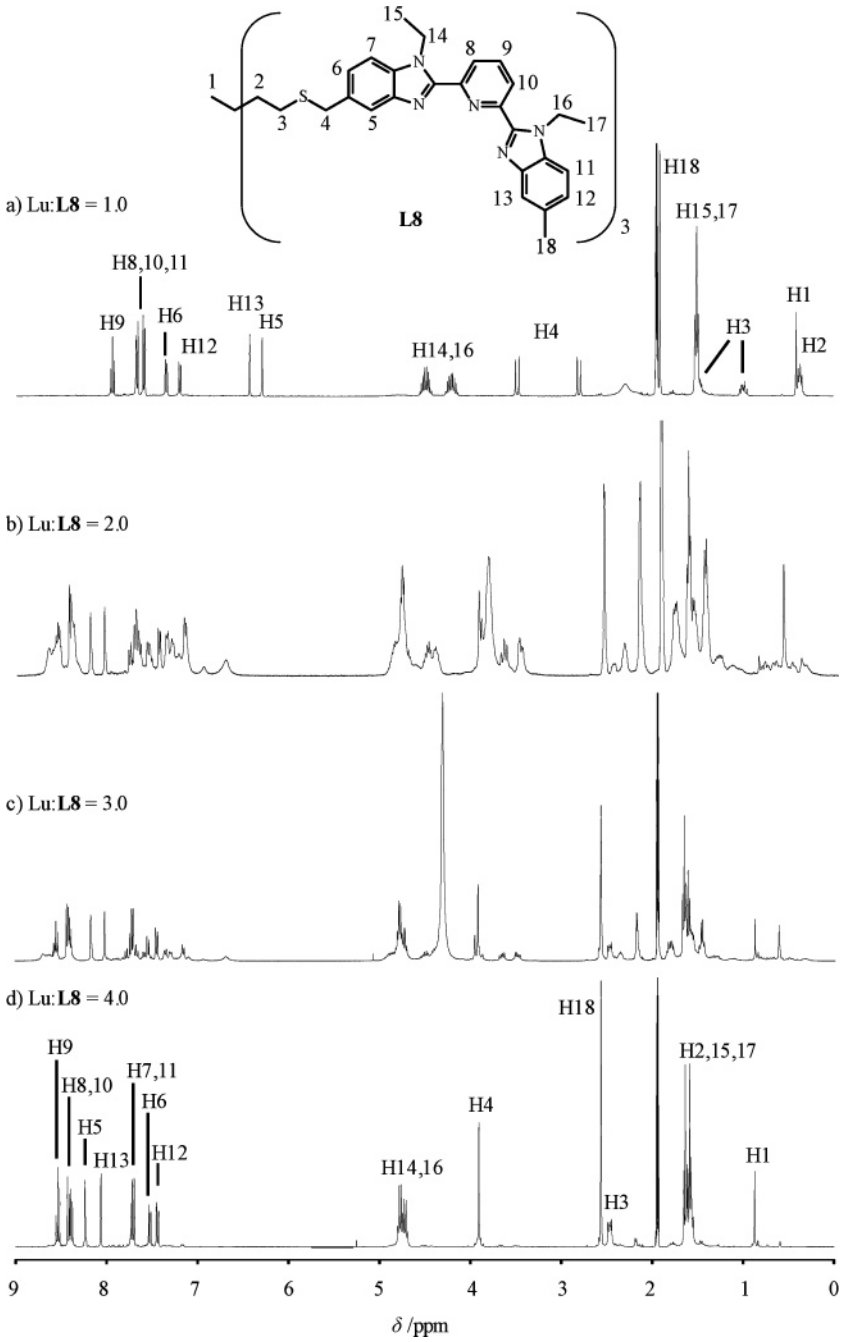

Figure 9. ^{1}H NMR spectra recorded during the titration of **L8** with $Lu(CF_3SO_3)_3 \cdot 1.6H_2O$ for (a) Lu:**L8** = 1.0, (b) Lu:**L8** = 2.0, (c) Lu:**L8** = 3.0 and (d) Lu:**L8** = 4.0 ($|\mathbf{L8}|_{tot} = 10^{-2}$ M, CD_3CN, 298 K).

boxylic acid monomethyl ester (**4**, 1.99 g, 11 mmol), CH_2Cl_2 (25 mL), thionyl chloride (7.7 mL, 110 mmol, 10 equiv), and DMF (10 μL) were refluxed for 1.5 h under nitrogen and evaporated to dryness. The white residue was dried under vacuum for 1 h and dissolved in CH_2Cl_2 (10 mL), and a solution of ethyl-(4-methyl-2-nitro-phenyl)-amine (**2**, 1.8 g, 10 mmol) and triethylamine (1.5 mL, 11 mmol) in CH_2Cl_2 (15 mL) was added dropwise. The resulting mixture was strirred at room temperature for 30 min, refluxed for 1 h, successively washed with aq. sat. $NaHCO_3$ (2 × 20 mL) and aq. sat. NH_4Cl (1 × 20 mL), dried over $MgSO_4$, and evaporated to yield a brown oil, which was purified by column chromatography (silicagel, CH_2Cl_2/MeOH 100:0 → 97:3) to afford **5** as a brown-orange oil (3.3 g, 9.6 mmol, 96%). ^{1}H NMR ($(CD_3)_2SO$, 440 K): δ = 1.80 (t, ^3J = 7.1 Hz, 3H; CH_3(Et)), 2.37 (s, 3H; Ar−CH_3), 3.50−4.16 (m, 5H; CH_2 (Et) and OCH_3), 7.34 (d, ^3J = 7.2 Hz, 1H; Ar−H), 7.47 (d, ^3J = 8.2 Hz, 1H; Ar−H), 7.80 (s, 1H; Ar−H), 7.85−7.90 (m, 2H; Ar−H), 7.97 ppm (d, ^3J = 7.2 Hz, 1H; Ar−H); ESI-MS (CH_2Cl_2/MeOH 9:1): 344.1 [M + H$^+$].

Preparation of 6-[Ethyl-(4-methyl-2-nitro-phenyl)-carbamoyl]-pyridine-2-carboxylic Acid (6). A solution of $LiOH \cdot H_2O$ (2.1 g, 50 mmol) in methanol (40 mL) and water (20 mL) was added dropwise to a solution of 6-[ethyl-(4-methyl-2-nitro-phenyl)-carbamoyl]-pyridine-2-carboxylic acid methyl ester (**5**, 3.43 g, 10 mmol) in methanol (20 mL) at 0 °C. The resulting mixture was stirred for 3 h at 0 °C, diluted with water (400 mL), and washed with CH_2Cl_2 (3 × 25 mL). The pH of the aqueous phase was adjusted to 2 with concentrated hydrochloric acid (37%). The solution was extracted with CH_2Cl_2 (4 × 40 mL), and the combined organic phases were dried over $MgSO_4$ and evaporated to dryness to afford **6** as a yellow solid (3.23 g, 9.8 mmol, 98%). ^{1}H NMR ($CDCl_3$): δ = 1.28 (t, ^3J = 7.2 Hz, 3H; CH_3(Et)), 2.44 (s, 3H;

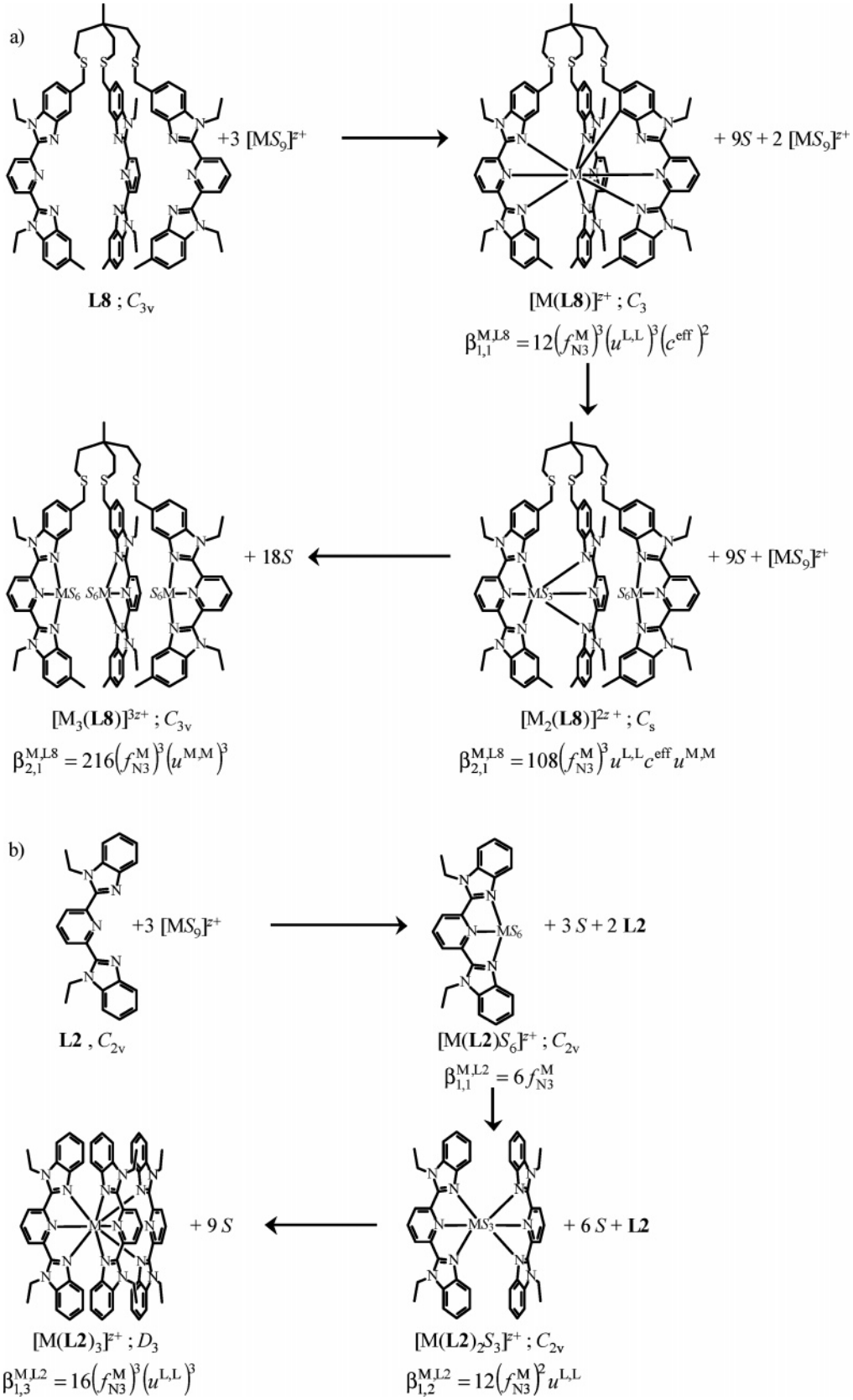

Figure 10. Successive complexation reactions leading to (a) $[M_m(\mathbf{L8})]^{zm+}$ ($z = 2$, 3 and $m = 1-3$) and (b) $[M(\mathbf{L2})_n]^{z+}$ ($z = 2$, 3 and $n = 1-3$) with thermodynamic formation constants modeled with eq 2 ($S = CH_3CN$).[22,24] The statistical factors $\omega_{m,n}^{\text{chiral}} \cdot \omega_{m,n}^{\text{M,L}}$ are calculated in Figure S4 (Supporting Information).[23]

Ar−CH_3), 3.82 (sext, $^3J = 7.2$ Hz, 1H; CH (Et)), 4.18 (sext, $^3J = 7.2$ Hz, 1H; CH (Et)), 7.28 (d, $^3J = 8.1$ Hz, 1H; Ar−H), 7.43 (dd, $^3J = 8.1$ Hz, $^4J = 1.4$ Hz, 1H; Ar−H), 7.68 (d, $^4J = 1.4$ Hz, 1H; Ar−H), 8.00 (t, $^3J = 7.8$ Hz, 1H; Ar−H), 8.12 (dd, $^3J = 7.8$ Hz, $^4J = 1.0$ Hz, 1H; Ar−H), 8.20 ppm (dd, $^3J = 7.8$ Hz, $^4J = 1.0$ Hz, 1H; Ar−H); ESI-MS (CH_2Cl_2/MeOH 9:1): 330.5 [M + H^+].

Table 4. Fitted Microscopic Thermodynamic Parameters for $[M_m(\mathbf{L8})]^{mz+}$ ($m = 1, 2$, $z = 2, 3$) and $[M(\mathbf{L2})_n]^{z+}$ ($n = 1-3$, $z = 2, 3$; Simultaneous Linear Least-Squares Fits of Eqs 11, 14−16, Acetonitrile + 0.01 M $(^nBu)_4NClO_4$, 298 K)[a]

microscopic parameters	Ca	La	Eu	Lu	Lu[b]
$\log(f^{M}_{N3})/\Delta G^{M}_{inter}$ (kJ/mol)	3.8(2)/−21(1)	6.3(2)/−35(1)	8.7(3)/−49(2)	9.15(8)/−51.3(5)	9.15(8)/−51.3(5)
$\log(f^{M}_{N3} \cdot c^{eff})/\Delta G^{M}_{intra}$ (kJ/mol)	2.2(4)/−12(4)	1.5(2)/−8(1)	1.4(2)/−8(1)	1.52(8)/−8.5(4)	1.52(8)/−8.5(4)
$\log(c^{eff})/\Delta G^{M}_{corr}$ (kJ/mol)	−1.6(2)/9(1)	−4.8(2)/27(1)	−7.3(3)/39(2)	−7.63(8)/42.8(4)	−7.63(8)/42.8(4)
$\log(u^{L,L})/\Delta E^{L,L}$ (kJ/mol)	−0.2(2)/1(1)	−0.9(2)/5(1)	−1.8(3)/10(2)	−1.74(9)/9.8(5)	−1.74(9)/9.8(5)
$\log(u^{M,M})/\Delta E^{M,M}$ (kJ/mol)	–	–	–	–	−7.4(2)/42(1)
AF[c]	0.014	0.012	0.012	0.003	0.003

[a] The uncertainties correspond to those obtained during the multilinear least-square fit processes. [b]Fitted with eqs 11, 12, 14−16; see text. [c]Agreement factor $AF = \sqrt{(\sum_i(\log(\beta_i^{exp})-\log(\beta_i^{calcd}))^2)/(\sum_i(\log(\beta_i^{exp}))^2)}$.

Preparation of Pyridine-2,6-dicarboxylic Acid 2-[Ethyl-(4-methoxymethyl-2-nitro-phenyl)-amide] 6-[Ethyl-(4-methyl-2-nitro-phenyl)-amide] (9). A mixture of 6-[ethyl-(4-methyl-2-nitro-phenyl)-carbamoyl]-pyridine-2-carboxylic acid (**6**, 0.68 g, 2.1 mmol), CH_2Cl_2 (5 mL), thionyl chloride (1.4 mL, 20 mmol, 10 equiv) and DMF (10 μL) was refluxed for 1.5 h under a nitrogen atmosphere and evaporated to dryness. The yellow residue was dried under vacuum for 1 h and then dissolved in CH_2Cl_2 (3 mL). A solution of ethyl-(4-methoxymethyl-2-nitro-phenyl)amine (**8**, 0.42 g, 2.0 mmol) and triethylamine (0.3 mL, 2.0 mmol) in CH_2Cl_2 (3 mL) was then added dropwise. The mixture was stirred at room temperature for 30 min, refluxed for 1 h washed with aq. half-sat. NH_4Cl (2 × 10 mL), dried over $MgSO_4$, and evaporated to yield a brown oil, which was purified by column chromatography (silicagel, CH_2Cl_2/MeOH 100:0 → 97:3) to afford **9** as a beige solid (1.0 g, 1.9 mmol, 96%). ^{1}H NMR ($(CD_3)_2SO$, 440 K): $\delta = 1.10$ (m, 6H; CH_3(Et)), 2.37 (s, 3H; Ar−CH_3), 3.34 (m, 3H; OCH_3), 3.70 (m, 4H; CH_2(Et)), 4.48 (s, 2H; Ar−CH_2O), 7.27 (m, 1H; Ar−H), 7.38 (m, 1H; Ar−H), 7.46−7.48 (m, 3H; Ar−H), 7.62 (d, $^3J = 7.0$ Hz, 1H; Ar−H), 7.75 (s, 1H; Ar−H), 7.81 (m, 1H; Ar−H), 7.87 ppm (s, 1H; Ar−H); ESI-MS (CH_2Cl_2/MeOH 9:1): 522.5 [M + H$^+$].

Preparation of 6-(1-Ethyl-5-methoxymethyl-1*H*-benzoimidazol-2-yl)-2-(1-ethyl-5-methyl-1*H*-benzoimidazol-2-yl)-pyridine (10). To a solution of pyridine-2,6-dicarboxylic acid 2-[ethyl-(4-methoxymethyl-2-nitro-phenyl)-amide] 6-[ethyl-(4-methyl-2-nitro-phenyl)-amide] (**9**, 2.48 g, 4.75 mmol) in ethanol/water (315 mL/95 mL), activated iron powder (4.25 g, 75.8 mmol) and concentrated hydrochloric acid (37%, 11.6 mL, 138.6 mmol) were added. The mixture was refluxed for 18 h under nitrogen, the excess of iron was filtered off, and ethanol was distilled under vacuum. The resulting mixture was poured into CH_2Cl_2 (100 mL), $Na_2H_2EDTA \cdot 2H_2O$ (51 g, 137 mmol) in water (250 mL) was added, and the resulting stirred mixture was neutralized (pH 7.0) with concentrated aqueous NH_4OH solution. Concentrated H_2O_2 solution (30%, 2.7 mL, 27 mmol) was added under vigorous stirring, and the pH was adjusted to 8.5 with aqueous NH_4OH solution. After 15 min, the organic layer was separated and the aqueous phase was extracted with CH_2Cl_2 (3 × 50 mL). The combined organic phases were washed with water until neutral, dried over Na_2SO_4, and evaporated to dryness. The crude residue was purified by column chromatography (silicagel, CH_2Cl_2/MeOH 100:0 → 97:3) to afford **10** as a white solid (1.93 g, 4.53 mmol, 95%). ^{1}H NMR ($CDCl_3$): $\delta = 1.37$ (t, $^3J = 7.2$ Hz, 3H; CH_3 (Et)), 1.38 (t, $^3J = 7.2$ Hz, 3H; CH_3 (Et)), 2.55 (s, 3H; Ar−CH_3), 3.44 (s, 3H; OCH_3), 4.65 (s, 2H; Ar−CH_2O), 4.81 (m, 4H; CH_2 (Et)), 7.22 (dd, $^3J = 8.3$ Hz, $^4J = 1.4$ Hz, 1H; Ar−H), 7.40 (m, 2H; Ar−H), 7.49 (d, $^3J = 8.3$ Hz, 1H; Ar−H), 7.68 (s, 1H; Ar−H), 7.84 (s, 1H; Ar−H), 8.07 (t, $^3J = 7.9$ Hz, 1H; Ar−H), 8.36 ppm (m, 2H; Ar−H); ESI-MS (CH_2Cl_2/MeOH 9:1): 426.0 [M + H$^+$].

Preparation of {1-Ethyl-2-[6-(1-ethyl-5-methyl-1*H*-benzoimidazol-2-yl)-pyridin-2-yl]-1*H*-benzoimidazol-5-yl}-methanol (11). A mixture of 6-(1-ethyl-5-methoxymethyl-1*H*-benzoimidazol-2-yl)-2-(1-ethyl-5-methyl-1*H*-benzoimidazol-2-yl)-pyridine (**10**, 0.6 g, 1.4 mmol) in acetic anhydride/CH_2Cl_2 (10 mL/10 mL) and $BF_3 \cdot Et_2O$ (0.9 mL, 7 mmol) was stirred for 16 h at room temperature and poured into an ice-cooled aq. 1 M KOH (400 mL). The aqueous layer was extracted with CH_2Cl_2 (2 × 10 mL). The combined organic phases were washed with deionized water until neutral, dried over Na_2SO_4, filtered, and evaporated to dryness to afford the crude acetate, which was dissolved in methanol (80 mL) and aq. 1 M KOH (50 mL) and stirred for 15 h at room temperature. The methanol was distilled under vacuum, and the resulting solution was poured into brine (150 mL) and extracted with CH_2Cl_2 (4 × 30 mL). The combined organic phases were washed with deionized water until neutral, dried over $MgSO_4$, filtered, and evaporated to dryness. The resulting crude compound was purified by column chromatography (silicagel, CH_2Cl_2/MeOH 98:2 → 94:6) to afford **11** as a white solid (0.57 g, 1.38 mmol, 99%). ^{1}H NMR ($CDCl_3$): $\delta = 1.37$ (t, $^3J = 7.2$ Hz, 3H; CH_3 (Et)), 1.39 (t, $^3J = 7.2$ Hz, 3H; CH_3 (Et)), 2.55 (s, 3H; Ar−CH_3), 4.79 (q, $^3J = 7.2$ Hz, 2H; CH_2 (Et)), 4.81 (q, $^3J = 7.2$ Hz, 2H; CH_2 (Et)), 4.86 (s, 2H; Ar−CH_2O), 7.22 (dd, $^3J = 8.3$ Hz, $^4J = 1.4$ Hz, 1H; Ar−H), 7.39 (d, $^3J = 8.3$ Hz, 1H; Ar−H), 7.43 (dd, $^3J = 8.3$ Hz, $^4J = 1.4$ Hz, 1H; Ar−H), 7.48 (d, $^3J = 8.3$ Hz, 1H; Ar−H), 7.69 (s, 1H; Ar−H), 7.82 (s, 1H; Ar−H), 8.01 (t, $^3J = 7.9$ Hz, 1H; Ar−H), 8.31 ppm (d, $^3J = 7.9$ Hz, 2H; Ar−H); ESI-MS (CH_2Cl_2/MeOH 9:1): 412.5 [M + H$^+$].

Preparation of 6-(5-Chloromethyl-1-ethyl-1*H*-benzoimidazol-2-yl)-2-(1-ethyl-5-methyl-1*H*-benzoimidazol-2-yl)-pyridine (12). A mixture of {1-ethyl-2-[6-(1-ethyl-5-methyl-1*H*-benzoimidazol-2-yl)-pyridin-2-yl]-1*H*-benzoimidazol-5-yl}-methanol (**11**, 1.02 g, 2.48 mmol), CH_2Cl_2 (40 mL) and thionyl chloride (1.8 mL, 25 mmol) was stirred for 16 h at room temperature; it was then poured into aq. sat. $NaHCO_3$ (400 mL). The aqueous layer was extracted with CH_2Cl_2 (3 × 20 mL), and the combined organic phases were washed with deionized water until neutral, dried over $MgSO_4$, filtered, and evaporated to dryness. The resulting crude compound was purified by column chromatography (silicagel, CH_2Cl_2/MeOH 100:0 → 98:2) to afford **12** as a white solid (0.89 g, 2.07 mmol, 83%). ^{1}H NMR ($CDCl_3$): $\delta = 1.38$ (t, $^3J = 7.2$ Hz, 3H; CH_3 (Et)), 1.39 (t, $^3J = 7.2$ Hz, 3H; CH_3 (Et)), 2.55 (s, 3H; Ar−CH_3), 4.80 (m, 4H; CH_2 (Et)), 4.82 (s, 2H; Ar−CH_2Cl), 7.23 (dd, $^3J = 8.4$ Hz, $^4J = 1.1$ Hz, 1H; Ar−H), 7.39 (d, $^3J = 8.4$ Hz, 1H; Ar−H), 7.45 (dd, $^3J = 8.4$ Hz, $^4J = 1.6$ Hz, 1H; Ar−H), 7.50 (d, $^3J = 8.4$ Hz, 1H; Ar−H), 7.69 (s, 1H; Ar−H), 7.89 (s, 1H; Ar−H), 8.08 (t, $^3J = 7.9$ Hz, 1H; Ar−H), 8.34 (dd, $^3J = 7.9$ Hz, $^4J = 1.0$ Hz, 1H; Ar−H), 8.38 ppm (d, $^3J = 7.9$ Hz, 1H; Ar−H); ESI-MS (CH_2Cl_2/MeOH 9:1): 430.4 [M + H$^+$].

Preparation of Thioacetic Acid *S*-{1-Ethyl-2-[6-(1-ethyl-5-methyl-1*H*-benzoimidazol-2-yl)-pyridin-2-yl]-1*H*-benzoimidazol-5-ylmethyl} Ester (13). 6-(5-Chloromethyl-1-ethyl-1*H*-benzoimidazol-2-yl)-2-(1-ethyl-5-methyl-1*H*-benzoimidazol-2-yl)-pyridine (**12**, 500 mg, 1.16 mmol) was dissolved in a suspension of potassium thioacetate (797 mg, 6.97 mmol, 6 equiv) in acetone (15 mL) and dichloromethane (15 mL). The mixture was stirred and heated at 55 °C for 16 h and then evaporated to dryness. The resulting solid was dissolved in ethyl acetate (20 mL) and water (20 mL). The aqueous phase was separated and extracted with ethyl acetate (2 × 30 mL). The combined organic phases were washed with brine, dried over Na_2SO_4, and evaporated to yield a

pale yellow viscous oil, which was purified by column chromatography (silicagel, CH_2Cl_2/MeOH 98:2) to afford **13** as a white solid (523 mg, 1.14 mmol, 96%). ^{1}H NMR ($CDCl_3$): $\delta = 1.34$ (t, $^3J = 7.2$ Hz, 6H; CH_3(Et)), 2.36 (s, 3H; Ar−CH_3), 2.52 (s, 3H; CH_3CO), 4.31 (s, 2H; Ar−CH_2), 4.73−4.80 (m, 4H; CH_2(Et)), 7.19 (d, $^3J = 8.3$ Hz, 1H; CH), 7.30 (dd, $^3J = 8.4$ Hz, $^4J = 1.0$ Hz, 1H; CH), 7.36 (d, $^3J = 8.3$ Hz, 1H; CH), 7.40 (d, $^3J = 8.4$ Hz, 1H; CH), 7.65 (s, 1H; CH), 7.78 (s, 1H; CH), 8.04 (t, $^3J = 7.9$ Hz, 1H; CH), 8.30 (dd, $^3J = 7.9$ Hz, $^4J = 1.0$ Hz, 1H; CH), 8.33 ppm (d, $^3J = 7.9$ Hz, 1H; CH); ESI-MS (CH_2Cl_2/MeOH 9:1): 470.9 [M + H$^+$].

Preparation of {1-Ethyl-2-[6-(1-ethyl-5-methyl-1*H*-benzoimidazol-2-yl)-pyridin-2-yl]-1*H*-benzoimidazol-5-yl}-methanethiol (14). Thioacetic acid *S*-{1-ethyl-2-[6-(1-ethyl-5-methyl-1*H*-benzoimidazol-2-yl)-pyridin-2-yl]-1*H*-benzoimidazol-5-ylmethyl} ester (**13**, 310 mg, 0.66 mmol) was dissolved in methanol (46 mL) and concentrated HCl (37%, 4 mL). The mixture was stirred and heated at 45 °C for 16 h. The methanol was then evaporated, and ethyl acetate (20 mL), water (20 mL), and aq. sat. $NaHCO_3$ (20 mL) were added to the resulting solution. The aqueous phase was separated and extracted with ethyl acetate (2 × 30 mL). The combined organic phases were washed with brine, dried over Na_2SO_4, and evaporated to yield a pale yellow viscous oil, which was purified by column chromatography (silicagel, CH_2Cl_2/MeOH 98:2) to afford **14** as a white solid (278 mg, 0.65 mmol, 99%). ^{1}H NMR ($CDCl_3$): $\delta = 1.35$ (m, 6H; CH_3(Et)), 1.82 (t, $^3J = 7.4$ Hz, 1H; SH), 2.52 (s, 3H; Ar−CH_3), 3.92 (d, $^3J = 7.4$ Hz, 2H; Ar−CH_2), 4.76 (m, 4H; CH_2(Et)), 7.19 (d, $^3J = 8.3$ Hz, 1H; CH), 7.35 (d, $^3J = 8.3$ Hz, 2H; CH), 7.42 (d, $^3J = 8.3$ Hz, 1H; CH), 7.65 (s, 1H; CH), 7.78 (s, 1H; CH), 8.03 (t, $^3J = 7.90$ Hz, 1H; CH), 8.32 ppm (t, $^3J = 7.90$ Hz, 2H; CH); ESI-MS (CH_2Cl_2/MeOH 9:1): 428.5 [M + H$^+$].

Preparation of L8. {1-Ethyl-2-[6-(1-ethyl-5-methyl-1*H*-benzoimidazol-2-yl)-pyridin-2-yl]-1*H*-benzoimidazol-5-yl}-methanethiol (**14**, 1.67 g, 3.91 mmol, 4 equiv) and 1,5-dichloro-3-(2-chloro-ethyl)-3-methyl-pentane (19, 213 mg, 0.98 mmol, 1 equiv) were dissolved in a suspension of dry cesium carbonate (1.27 g, 3.91 mmol, 4 equiv) in freshly distilled DMF (50 mL) under a nitrogen atmosphere. The mixture was stirred, heated at 60 °C for 16 h, filtered, and evaporated to dryness. The resulting solid was dissolved in dichloromethane (100 mL) and brine (50 mL). The organic phase was washed with water (50 mL) and brine (50 mL), dried over Na_2SO_4, and evaporated to dryness to yield a solid, which was purified by column chromatography (silicagel, CH_2Cl_2/MeOH 98:2 → 96:4) to afford **L8** as a white solid (1.05 g, 0.75 mmol, 77%). ^{1}H NMR ($CDCl_3$): $\delta = 0.77$ (s, 3H; H^1), 1.30−1.35 (m, 18H; H^{15,17}), 1.41−1.45 (m, 6H; H^2), 2.27−2.31 (m, 6H; H^3), 2.52 (s, 9H; H^{18}), 3.81 (s, 6H; H^4), 4.73 (q, $^3J = 7.0$ Hz, 12H; H^{14,16}), 7.18 (dd, $^3J = 8.3$ Hz, $^4J = 1.0$ Hz, 3H; H^{12}), 7.30 (dd, $^3J = 8.4$ Hz, $^4J = 1.3$ Hz, 3H; H^6), 7.33 (d, $^3J = 8.3$ Hz, 3H; H^{11}), 7.37 (d, $^3J = 8.4$ Hz, 3H; H^7), 7.64 (s, 3H; H^{13}), 7.74 (s, 3H; H^5), 7.99 (t, $^3J = 7.8$ Hz, 3H; H^9), 8.33−8.39 ppm (m, 6H; H^{8,10}); ESI-MS (CH_2Cl_2/MeOH 9:1): 1391.3 [M + H$^+$], 696.3 [M + 2H$^+$]. $C_{83}H_{87}N_{15}S_3$·0.5H_2O (1399.9) calcd: C, 71.21, H, 6.34; N, 15.00. found: C, 71.02; H, 6.33; N, 14.90.

Preparation of the Complexes [Ca(L8)](CF_3SO_3)$_2$·3H_2O and [Ln(L8)](CF_3SO_3)$_3$·*x*H_2O (Ln = La, *x* = 4; Ln = Nd, *x* = 4; Ln = Eu, *x* = 4; Ln = Gd, *x* = 4; Ln = Tb, *x* = 3; Ln = Lu, *x* = 4; Ln = Y, *x* = 2). A solution of Ca(CF_3SO_3)$_2$·0.5H_2O or Ln(CF_3SO_3)$_3$·*x*H_2O (Ln = La, Nd, Eu, Gd, Tb, Lu, Y; 21 μmol) in acetonitrile (4 mL) was added to a solution of **L8**·0.5H_2O (30 mg, 21 μmol) in dichloromethane (4 mL). The resulting pale yellow mixture was evaporated to dryness. The residue was dissolved in acetonitrile, and diethyl ether was added to precipitate the complex. The resulting pale yellow powders were collected by filtration and dried to give [Ca(**L8**)](CF_3SO_3)$_2$·3H_2O and [Ln(**L8**)](CF_3SO_3)$_3$·*x*H_2O (Ln = La, *x* = 4; Ln = Nd, *x* = 4; Ln = Eu, *x* = 4; Ln = Gd, *x* = 4; Ln = Tb, *x* = 3; Ln = Lu, *x* = 4; Ln = Y, *x* = 2) in 69−94% yield. All the complexes gave satisfying elemental analyses (Table S2, Supporting Information), ESI-MS and NMR spectra. X-ray quality plates of [Eu(**L8**)](ClO_4)$_3$·2CH_3CN·C_2H_5OH·0.5H_2O (**20**) were obtained by slow diffusion of *tert*-butylmethylether into a concentrated solution of [Eu(**L8**)](CF_3SO_3)$_3$·4H_2O in acetonitrile/ethanol (99.9:0.1) containing (^{n}Bu)$_4$$NClO_4$ (3 equiv).

Table 5. Summary of Crystal Data, Intensity Measurement, and Structure Refinement for [Eu(**L8**)](ClO_4)$_3$·2CH_3CN·C_2H_5OH·0.5H_2O (**20**)

formula	$C_{89}H_{100}Cl_3EuN_{17}O_{13.5}S_3$
fw	1978.6
crystal system	monoclinic
space group	$P2_1/c$
a (Å)	14.4595 (6)
b (Å)	15.5595 (5)
c (Å)	43.521 (1)
α (deg)	90
β (deg)	96.035 (5)
γ (deg)	90
V (Å^3)	9737.2 (7)
Z	4
crystal size (mm^3)	0.048 × 0.21 × 0.26
d_{calcd} (g·cm^{-3})	1.350
μ(Mo Kα) (mm^{-1})	0.858
T_{min}, T_{max}	0.8561, 0.9594
2*θ* max (deg)	51.8
no. of reflns collected	78259
no. of independent reflns	19010
criterion (*q*) for obsd reflns^{a,b}	4
no. of obsd^a (used^b) reflns	8832 (9465)
no. of variables	1188
weighting scheme p^c	0.0002
max and min Δ*ρ* (e Å^{-3})	1.60, −1.86
GOF ^{d} (all data)	1.37(1)
R^e, ωR^f	0.050, 0.049

^{a} $|F_o| > q\,\sigma(F_o)$. ^{b}Used in the refinements (including reflns with $|F_o| \leq q\,\sigma(F_o)$ if $|F_c| > |F_o|$). $^c\omega = 1/[\sigma^2(F_o) + p(F_o)^2]$. $^dS = [\sum\{((F_o - F_c)/\sigma(F_o))^2\}/(N_{ref} - N_{var})]^{1/2}$. $^eR = \sum||F_o| - |F_c|/\sum|F_o|$. $^f\omega R = [\sum(\omega|F_o| - |F_c|/\sum\omega|F_o|^2]^{1/2}$.

Single-Crystal Structure Determination. Summary of crystal data, intensity measurements, and structure refinements for [Eu(**L8**)](ClO_4)$_3$·2CH_3CN·C_2H_5OH·0.5H_2O (**20**) were collected in Table 5. The crystal was mounted on a quartz fiber with protection oil. Cell dimensions and intensities were measured at 150 K on a Stoe IPDS diffractometer with graphite-monochromated Mo Kα radiation (λ = 0.710 73 Å). Data were corrected for Lorentz and polarization effects and for absorption. The structure was solved by direct methods (SIR97),[40] and all other calculation were performed with the XTAL[41] system and ORTEP[42] programs. CCDC-658414 contains the supplementary crystallographic data for **20**. The perchlorates e and f were disordered and refined with restraints on bond distances and bond angles. Two oxygen atoms of the perchlorate were refined on two sites with population parameters of 0.65/0.35 and 0.6/0.4, respectively. Both molecules of ethanol and the water molecule were refined with population parameters of 0.5, 0.5, and 0.25, respectively, and the atomic positions of the hydrogen atoms of these molecules were not calculated. For all the other atoms, the atomic positions of the hydrogen atoms were calculated. The cif files can be obtained free of charge via www.ccdc.cam.ac.uk/conts/retrieving.html (or from the Cambridge Crystallographic Data Centre, 12 Union Road, Cambridge CB2 1EZ, UK; fax: (+44) 1223-336-033; or deposit@ccdc.cam.ac.uk).

Spectroscopic and Analytical Measurements. Electronic spectra in the UV−vis were recorded at 20 °C from solutions in CH_3CN with a Perkin-Elmer Lambda 900 spectrometer using quartz cells of 0.1 or 1 mm path length. Spectrophotometric titrations were performed with a J&M diode array spectrometer (Tidas series) connected to an external

(40) Altomare, A.; Burla, M. C.; Camalli, M.; Cascarano, G.; Giacovazzo, C.; Guagliardi, A.; Moliterni, G.; Polidori, G.; Spagna, R. *J. Appl. Crystallogr.* **1999**, *32*, 115−119.
(41) *XTAL 3.2 User's Manual*; Hall, S. R., Flack, H. D., Stewart, J. M., Eds.; Universities of Western Australia and Maryland, 1989.
(42) Johnson, C. K. O*RTEP II; Report ORNL-5138*; Oak Ridge National Laboratory: Oak Ridge, Tennessee, 1976.

computer. In a typical experiment, 25 mL of **L8** (10^{-4} M) in CH_3CN + 10^{-2} M $(^nBu)_4NClO_4$ were titrated at 20 °C with a solution of $Ca(CF_3SO_3)_2 \cdot 0.5H_2O$ or $Ln(CF_3SO_3)_3 \cdot xH_2O$ (10^{-3} M) in the same solvent under an inert atmosphere. After each addition of 0.10 mL, the absorbance was recorded using Hellma optrodes (optical path length 0.1 cm) immersed in the thermostated titration vessel and connected to the spectrometer. Mathematical treatment of the spectrophotometric data was performed with factor analysis[43] and with the SPECFIT program.[28] ^1H and ^{13}C NMR spectra were recorded at 25 °C on a Bruker Avance 400 MHz spectrometer. Chemical shifts are given in ppm with respect to TMS. Pneumatically assisted electrospray (ESI-MS) mass spectra were recorded from 10^{-4} M solutions on a Finnigan SSQ7000 instrument. Elemental analyses were performed by Dr. H. Eder from the microchemical Laboratory of the University of Geneva. Linear least-square fits were performed with Excel.

Conclusion

According to a structural point of view, the 25 synthetic steps required for connecting three tridentate N_3 binding units to a "strain-free" flexible covalent tripod are fully justified by the superimposable arrangements of the coordinated strands observed in $[Eu(\mathbf{L8})]^{3+}$ and $[Eu(\mathbf{L9})_3]^{3+}$. However, the latter concept turned to be a disaster for the complexation of nine-coordinate cations because of the very low effective concentrations ($10^{-7.6} \leq c^{eff} \leq 10^{-4.8}$ for Ln = La−Lu, Table 4), which prevent efficient intramolecular coordination processes. These values can be compared with $c^{eff} = 10^{-0.8}$ reported for the closely related but labile noncovalent tripod, promoting the formation of the polynuclear Eu(III) triple-stranded helicates $[Eu_3(\mathbf{L4})_3]^{9+}$ and $[Eu_4(\mathbf{L5})_3]^{12+}$.[22,33] Taking the preorganization of the labile tripods in $[Eu_3(\mathbf{L4})_3]^{9+}$ and $[Eu_4(\mathbf{L5})_3]^{12+}$ as reference, and assuming that both types of tripod (i.e., covalent in **L8** and noncovalent in the triple-stranded helicates) are flexible enough to use a $d^{-3/2}$ dependence of c^{eff} on the distance,[19] we predict on a pure entropic basis that $c^{eff} = (10^{-0.8}) \cdot (21/18)^{-3/2} = 10^{-0.9}$ for the intramolecular ring-closing reaction operating in $[Eu(\mathbf{L8})]^{3+}$ because the separation between two N_3 binding site connected by the labile tripod amounts to $2 \times 9 = 18$ Å in the triple-stranded helicates[22,24] and to ca. 21 Å in **L8**. The experimental value $c^{eff} \leq 10^{-7.3}$ is more than 6 orders of magnitude smaller, which unambigously indicates that, beyond obvious differences in the rigidity of the two types of tripods, some severe enthalpic constraints prevent the efficient complexation of Ln(III) in the final podate $[Eu(\mathbf{L8})]^{3+}$. Interestingly, the effective concentration observed in $[Ca(\mathbf{L8})]^{2+}$ ($c^{eff} = 10^{-1.6}$) fairly matches that predicted when the noncovalent tripod of triple-standed helicate is used as a reference for preorganization ($c^{eff} = 10^{-0.9}$). This drastic increase of c^{eff} in going from Ln^{3+} to Ca^{2+} is responsible for the unexpected large formation constant observed for $[Ca(\mathbf{L8})]^{2+}$, despite the limited electrostatic contribution brought by this bivalent cation. We thus suspect that the complexation of Ca(II) in the cavity of the podate $[Ca(\mathbf{L8})]^{2+}$, while conserving C_3-symmetry, is significantly different from that evidenced with Ln(III). We were however unable to obtain crystal structures with $[Ca(\mathbf{L8})]^{2+}$. Based on this reasoning, we conclude that c^{eff} is a crucial factor for quantitatively estimating (i) the preorganization of the receptor (either covalent or self-assembled) and (ii) its capicity to selectively complex a specific cation. Its drastic decrease related in the order Ca ≫ La > Eu ≈ Lu indicates that the receptor **L8** has a preference for large cations, with a special emphasis for Ca(II). On the other hand, its tighter wrapping about Eu(III) or Lu(III) disfavors the intramolecular processes to such an extent that competitive pathways, which minimize intramolecular events, can be detected with the formation of the polynuclear complexes $[Ln_2(\mathbf{L8})]^{6+}$ and $[Ln_3(\mathbf{L8})]^{9+}$. Since our thermodynamic analysis is quite general in its essence, the effective concentration c^{eff} can be considered as an efficient tool for estimating preorganization in any multicomponent assembly process. The correlation between molecular design and c^{eff} relies on intuitions derived from previous work on flexible polymers,[19] but no reliable concept can be currently proposed for its programming in assembly processes involving semirigid components. We however note that the use of flexible tripods compatible with the structural "strain-free" wrapping of the strands about the metal is misleading because the small entropic gain is overcome by considerable enthalpic constraints, which cannot be addressed in the analysis of the solid-state structures. Thermodynamic investigations of related systems with shorter and/or more rigid tripods are required to establish further trends and to improve a rational chemical programming of preorganization.

Acknowledgment. We thank P. Ryan for graphical representations of the complexes and P. Perrottet for carefully recording ESI-MS spectra. Financial support from the Swiss National Science Foundation is gratefully acknowledged.

Supporting Information Available: Data for structural and spectroscopic analyses (Tables S1−S6 and Figures S2, S3, and S5), for thermodynamic calculations (Table S7), and for statistical factors (Figures S1 and S4). Crystallographic data for the compound **20** in CIF format. This material is available free of charge via the Internet at http://pubs.acs.org.

JA0772290

(43) Malinowski, E. R.; Howery, D. G. *Factor Analysis in Chemistry*; Wiley: New York, Chichester, 1980.